Estimation of Relative Motion between Non-Rigid Bodies on a Semi-Truck

by

Brendan Schretter

A thesis submitted to the Graduate Faculty of
Auburn University
in partial fulfillment of the
requirements for the Degree of
Master of Science

Auburn, Alabama
December 9, 2023

Keywords: Extended Kalman Filter, GPS/INS, Allan Variance, Particle Filter, Semi-Truck

Approved by

David Bevly, Chair, Bill and Lana McNair Professor of Mechanical Engineering
Scott Martin, Assistant Research Professor of Mechanical Engineering
Chad Rose, Assistant Professor of Mechanical Engineering

Abstract

This thesis develops methods to estimate the relative motion between the cabin and chassis of a semi-truck without the use of a complex suspension model between the two bodies. In, this thesis only sensors that would be already available on current vehicle using both inertial and GPS sensors on the cabin and chassis bodies are utilized. Automation of Semi-Trucks requires perceiving obstacles that are both stationary and moving that exist close to the truck. The cabin and chassis of a truck have a suspension system between them. This can cause there to be offsets between the perception of obstacles from the cabin vs the chassis which can inhibit autonomy of the vehicle.

The thesis analyzes both the use of GPS/INS integration as well as Transfer Alignment techniques to correct an IMU mounted on the chassis with measurements taken from GPS antennas and IMUs mounted on the cabin. Additional methods are investigated to further improve these techniques such as taking into account the quality of the cabin measurements, adding higher fidelity models for state estimates, or reducing the amount of states. Using real world datasets, the methods are evaluated by comparing the corrected chassis solution to a high quality GPS/INS senor that acts as a truth measurement. The results show that the relative motion between the two bodies can be determined. The quality of the final solution is dependent on the performance of both the cabin solution and chassis IMU. The thesis will show with a high quality cabin GPS/INS solution the chassis attitude solution can be found to be within 0.5 degrees of the true value.

Acknowledgments

It has been amazing experience being apart of the GAVLAB (GPS and Vehicle Dynamics Lab) at Auburn University. I have a deep appreciation for the work my advisors Dr. Bevly and Dr. Martin do day in and day out at the lab to support us graduate students. I feel there was always both opportunities to work on real world problems through the sponsored work that they constantly bring in as well the support and backing from them when us students are continuing to go through the learning process. Thank you so much for helping me in my career.

The GAVLAB also brought me close to some of my best friends in life. Jake Ward, who will always be one of my best friends, was constantly there for me with advise and friendship ever since undergrad at Auburn. His dedication to getting people out to trivia nights at Sky Bar helped create some of my favorite memories! Will Bryan, Matt Boler, and Connor Jones who I got to enjoy beating in ping-pong and endless board game nights made each weekend something to look forward too! John David Sprunger, I appreciate greatly for all of his help on real-world sensor network help that would have taken me ages by myself.

I would like to thank my teammates on the Indy Autonomous Challenge. I feel the leadership and teamwork skills I learned through this competition are invaluable. Will is an incredibly confident leader who always stands with his teammates. Stephanie, who has one of the best work ethics and the competitive drive to always bounce back. Elizabeth made each day at the track more fun and made some of the best user interfaces for the car! Carson, Thomas, and Bryce for their dedication to the team and helping wherever needed! Your work did not go unnoticed!

Thank you to my mom and dad for their endless support. Whenever I was getting down on myself they could provide me with feed back to get me through anything. My sister, Katie for our long phone calls whenever we go on walks I know I could always reach out to for support in organizing my thoughts and life.

At the GAVLAB, I also met the love of my life Amy Strong, who is now my fiance! I am so excited to continue our life together and her support through this thesis process has been the most helpful!

”But those who hope in the Lord will renew their strength. They will soar on wings like eagles; they will run and not grow weary, they will walk and not be faint.” – Isaiah 40:31

Table of Contents

Abstract ii

Acknowledgments iii

List of Abbreviations xii

1 Introduction 1

1.1 Background and Motivation 1

1.2 Prior Research 3

1.3 Thesis Contributions 5

1.4 Thesis Outline 6

2 Technical Background 7

2.1 Coordinate Frames/Transformations 7

2.1.1 Earth-Centered Earth-Fixed Frame 7

2.1.2 Local Navigation Frame 8

2.1.3 Body Frame 8

2.1.4 Sensor Frame 8

2.1.5 Euler Angles 8

2.1.6 Direction Cosine Matrices 9

2.2 Inertial Mechanization 10

2.3 Gravity Terms 12

2.4 Kalman Filter 14

2.4.1 Extended Kalman Filter 15

3 Experimental Test Setup and Evaluation 18

3.1 Test Setup 18

3.2 Evaluation of Results 21

3.3 Location 21

3.4 Dataset 1: NCAT Track 22

3.5 Dataset 2: Roads 23

4 Dual GPS/INS using One GPS Antenna 25

4.1 Prediction Update 26

4.2 Measurement Update 29

4.3 Correction 30

4.4 Results 31

5 Transfer Alignment 34

5.1 Prediction Update 35

5.2 Measurement Update 37

5.3 Transfer Alignment Parameters 38

5.4 Results 39

5.5 Results Analysis 41

6 Transfer Alignment Improvements 45

6.1 Fault Detection 46

6.2 Rigidity Detection 47

6.3 Misalignment Models 49

6.3.1 Higher Order Markov Model 49

6.3.2 Flexure States 51

6.4 Measurement Noise related to Dynamic Motion 52

7 Dynamic Transfer Alignment 54

7.1 Results 54

7.1.1 Dynamic TA Stochastic Observability 57

7.1.2 Dynamic TA Deterministic Observability 59

7.2 Results Analysis 61

8 Reduced-Order Dynamic Transfer Alignment 63

8.1 Reduced Order Filter Design 64

8.2 Results 67

9 Conclusions and Future Work 73

9.1 Conclusions 73

9.2 Future Work 76

References 77

List of Figures

1.1 Cabin and Chassis Description 2

1.2 Attitude Errors Effect on Perception 2

1.3 Transfer Alignment Examples 4

2.1 WGS84 Ellipsoid representation of the Earth 12

2.2 Kalman Filter Visual [4] 14

2.3 Extended Kalman Filter Visual [4] 16

3.1 Truck Setup 19

3.2 Sensors 19

3.3 eTALIN Comparison 20

3.4 National Center for Asphalt Technology in Auburn, AL 21

3.5 Relative NED Velocity (Cabin minus Chassis) 22

3.6 Relative Attitude (Cabin minus Chassis) 22

3.7 Roads Location 23

3.8 True Relative Attitude (Cabin - Chassis) 24

3.9 True Relative Velocity (Cabin - Chassis) 24

4.1 Dual GPS/INS Method Block Diagram 25

4.2 Comparison between Dual GPS/INS Chassis Attitude and Chassis eTALIN Attitude 31

4.3 Error between GPS/INS Solution and Chassis eTALIN 32

4.4 Relationship between Velocity and Attitude Error States 33

4.5 NCAT Track highlighting Observability Challenges 33

5.1 Transfer Alignment Method Block Diagram 35

5.2 NCAT Attitude Transfer Alignment vs. Chassis eTALIN 40
5.3 NCAT Attitude Error Transfer Alignment vs. Chassis eTALIN 40
5.4 Roads Attitude Transfer Alignment vs. Chassis eTALIN 41
5.5 NCAT Dataset 41
5.6 Roads Dataset 42
5.7 NCAT Attitude Covariance 43
5.8 Zoomed-In NCAT Attitude Covariance 43
6.1 Fault Detection Example [12] 47
6.2 Initial NCAT Normalized Innovation Results 47
6.3 Rigid Body 48
6.4 NCAT Track Rigidity Detection 49
6.5 Example of Frequency Analysis [19] 50
6.6 Wing Rock Example [9] 51
6.7 Updated NCAT Normalized Innovation Results 53
7.1 NCAT Dynamic Attitude Covariance 55
7.2 NCAT Updated Transfer Alignment Attitude Covariances 56
7.3 NCAT Updated Transfer Alignment Misalignment Estimates 56
7.4 NCAT Updated Transfer Alignment Attitude Error Results 57
7.5 Stochastic Observability example when decreasing the quality of the reference system 58
7.6 Deterministic Observability Diagram 60
7.7 Roads Dataset Updated Transfer Alignment Attitude Error 60
7.8 Roads Dynamic Measurement Noise 61
8.1 NCAT Dataset Model-Reduced Dynamic Measurement Covariance Scaling . . 68
8.2 NCAT Dataset Model-Reduced Attitude Error 68
8.3 NCAT Dataset Model-Reduced Stability Concerns: Fault Detection 69

8.4 NCAT Dataset Model-Reduced Stability Concerns: Misalignment Angles . . . 70

8.5 NCAT Model-Reduced Updated Transfer Alignment Attitude Covariances . . . 70

8.6 Roads Model-Reduced Attitude Error 71

8.7 Roads Reduced Misalignment Angles 72

List of Tables

2.1 WGS84 Parameters. 13

3.1 Inertial Measurement Units Performance 19

3.2 GPS Receiver Solution Performance 20

3.3 eTALIN Solution Performance 20

5.1 Left: Initial Covariances, Right: Process Noise Parameters 38

5.2 Measurement Noise Parameters 39

List of Abbreviations

DCM Direction Cosine Matrix

ECEF Earth-Centered Earth-Fixed

EKF Extended Kalman Filter

ENU East-North-Up

IMU Inertial Measurement Unit

NED North-East-Down

WGS84 World Geodetic System 1984

Chapter 1

Introduction

1.1 Background and Motivation

The autonomous vehicle industry is an ever growing field with a recent focus on making semi-trucks autonomous. The trucking industry's total revenue for 2019 was around 700 billion dollars. Moreover, 13.4 percent of all vehicles are commercial trucks [24]. This industry alone handles over 70 percent of the nations goods [24]. Therefore, there is a large desire to save costs everywhere possible. Autonomy has the potential to help solve some of the industries biggest challenges such as fuel efficiency and driver shortages. In 2018, companies were short over 60,000 drivers for possible jobs which leads to massive loss in revenue [22].

This thesis focuses on the fact that semi-trucks have an additional suspension system between the cabin and the chassis that can cause an offset between the two frames. Figure 1.1a highlights the difference between the cabin and chassis bodies. The suspension system connecting the cabin and chassis often includes different kinds of springs, dampers, and anti-roll bars. These suspension components are used to create a comfortable ride for the driver under all road conditions. Figure 1.1b pictures a general model of a semi-truck that includes all these components. The unique suspension system creates difficulties in modelling the relative motion between the cabin and chassis, because of the sheer amount of components as seen in Figure 1.1b. Any model would need to include many variables for linear and angular spring-damper coefficients in all dimensions.

Nevertheless, knowledge of the motion of the cab (cabin) relative to the chassis is critical to making the truck autonomous. Key perception sensors are mounted to the cabin. However, if there is an offset between the cabin and chassis frame, then the chassis may "perceive" an

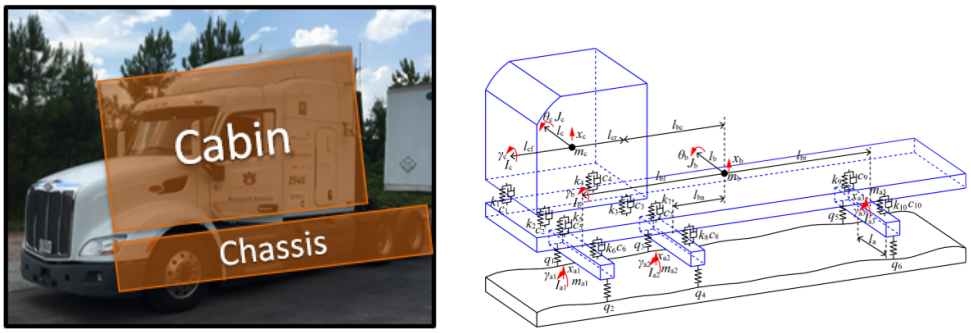

(a) Cabin and Chassis Example (b) Cabin and Chassis Diagram [3]

Figure 1.1: Cabin and Chassis Description

object to be offset from its true location. The truck suspension system allows the cab to be up to 3 degrees different from the chassis in the roll and pitch directions. This difference can negatively effect the path planning and control of the vehicle when using using the chassis as the main object to be controlled. Figure 1.2 demonstrates the impact that 1 - 3 degrees can have in the pitch and yaw directions. Being off by 3 degrees at the height of a semi-truck can misplace a detected object by 0.1 meters. This is unacceptable, as the absolute positioning needed for vehicles to maintain staying in a lane is around 0.1 meters. In fact, this number can be even lower for a semi-truck which are often wider than normal vehicles.

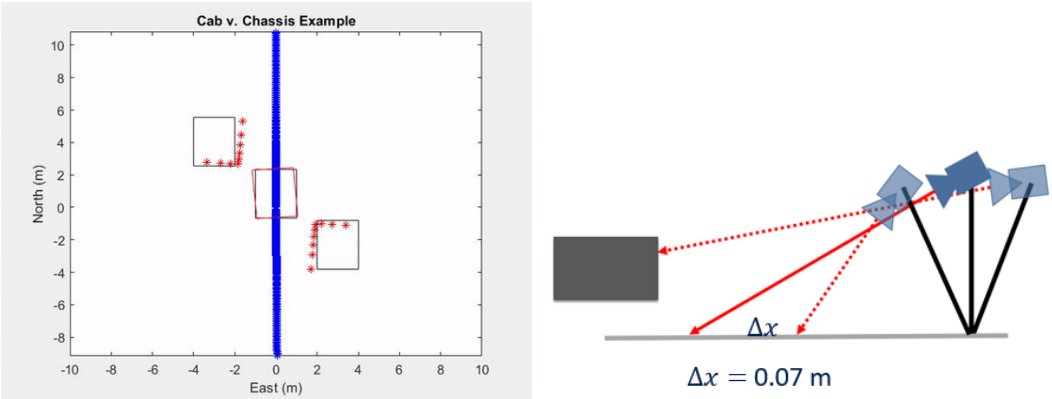

(a) Effect of Yaw Error (b) Effect of Pitch Error

Figure 1.2: Attitude Errors Effect on Perception

The problem of accounting for sensor motion may be solved by including many additional sensors to measure the difference between the cab and chassis such as range finders, LiDARS, or potentiometers. However, these sensors would add additional costs and may not be able to handle the harsh conditions of being under the truck body which often experiences dirt and

water while driving. Finally, these types of sensors may increase the amount of power and computation needed to properly calculate the relative motion of the two bodies.

This thesis addresses the issue by only using sensors that are already included on an autonomous semi-truck. An autonomous semi-truck could be assumed to be equipped with a GPS on the cabin body for absolute positioning and inertial systems are often equipped on both the cabin and chassis bodies for safety and local navigation uses. Therefore, the use of these sensors would not add any additional monetary cost and also these sensors are very robust in harsh working conditions. This thesis will look at overcoming the limited information that these sensors provide for estimating the relative motion between the cabin and chassis bodies.

1.2 Prior Research

This thesis utilizes algorithms that are common for localization in the autonomous vehicle world. The GPS/INS Extended Kalman filter (EKF) has been a popular form of positioning for many years and has been outlined thoroughly in many works including [10]. The GPS/INS EKF fuses the measurement outputs from the GPS and IMU and this helps overcome each of the sensors shortcomings. This fusion helps get the most out of each sensor. GPS reports absolute positioning with minimal variance and bias but is often slower, only reporting at around 1 Hz. However, the IMU can report at much faster rates (100-200Hz) and provide attitude information but can suffer from biases in its measurements which can cause large errors while integrating the accelerations. This thesis will expand on this GPS/INS sensor fusion to find the relative motion between the cabin and chassis bodies.

Estimation of relative motion has been very popular in the field of aerospace. Aircraft often have wing mounted systems that need to have very precise knowledge of their respective attitude but move frequently due to the flexibility of the wing. Research related to the topic of estimating relative motion was used to help initialize wing mounted devices on airplanes before their use. Similar to the truck cab motion, an aircraft using wing mounted sensors experiences motion relative to a reference mounted on the fuselage. Both the truck and the aircraft have a reference system and an accompanying IMU and there is no rigidity assumption between the two. Groves outlines different transfer alignment methods for optimising the performance

for use on an aircraft weapon INS system [8]. Rogers improves on the transfer alignment method by including angular-rate measurements as updates for the Kalman filter, known as rapid transfer alignment [17]. These techniques were then applied to additional systems such as ships and pedestrian navigation. Joon extended the rapid transfer alignment work by applying it to a large ship body to help estimate the large ship body flexures that can occur during travel [15]. Archit Thopay also applied transfer alignment methods to a foot-mounted IMU in a car by only applying the updates while the two bodies were considered rigid to one another, removing the need to estimate any misalignment between the two bodies [1]. Examples of Joon and Thopays setups are pictured in Figure 1.3. Additional methods attempted to find relative motion only using inertial measurements. Alan Schneider used only acceleration and gyroscope values to determine the dynamic misalignment angles between two bodies which were assumed to be in flexure [18]. The problem of estimating relative motion between two bodies is now a probelm for the autonomous semi-truck. This thesis extends the transfer alignment and GPS/INS work to the semi-truck cabin and chassis problem.

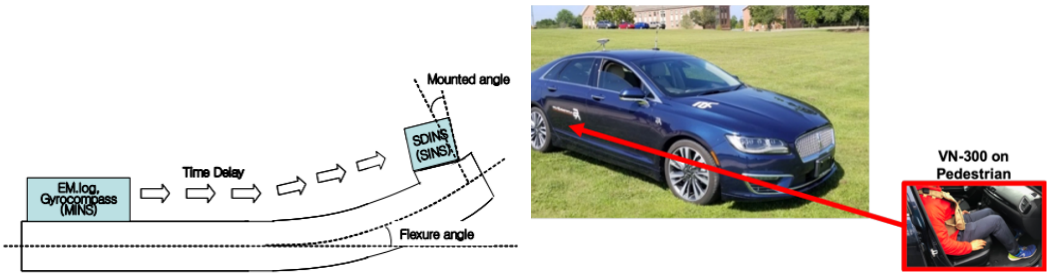

(a) Ship Flexure Setup [15] (b) Pedestrian Dead-Reckoning Initialization [1]

Figure 1.3: Transfer Alignment Examples

Further research related to the specific problem of relative motion between the cabin and chassis is outlined in a thesis by Edvin Agnas where the authors compare different motion models (separated bodies and merged bodies) to estimate the relative motion model between the cab and chassis while also comparing different sensor setups [2]. These models were based of rigid body dynamics and estimates both the cabin and chassis attitude in one combined filter. Agnas's work required the knowledge of a wide variety of parameters to be properly fitted to both the separated and merged body models. This thesis differs from Agnas's work by using

less sensors and attempting to estimate the relative motion without a complex motion model. Additionally, the focus of this thesis will be to rely on a main highly accurate cabin system to assist the simpler chassis system instead of estimating both cabin and chassis states at the same time.

1.3 Thesis Contributions

This thesis begins with an investigation and characterization of current sensor fusion techniques and applies them to the cabin and chassis system. Then the thesis will move to using sensor fusion methods that focus on systems that experience relative motion between their sensors and the main body of interest such as the Transfer Alignment method mentioned in Prior Research. Theses methods are then expanded by improving the observability and performance of those prior estimation techniques by reviewing many different potential additions or adaptations. All the solutions are tested on real world datasets that include both track and regular road driving and their performance is analyzed. The details of these contributions are listed below:

- Analyzed the use of a noncolocation GPS/INS integration using a GPS antenna on the cabin and the IMU located on the chassis
- Developed a Transfer Alignment filter for the semi-truck using a GPS/INS solution from the cabin to correct an IMU on the chassis
- Tested possible improvements to overcome observability and stability challenges such as rigidity detection, fault detection, and dynamic scaling of the measurement noise matrices
- Reviewed observability and stability of each algorithm
- Applied the transfer alignment algorithm and its improvements to real-world semi-truck datasets on both repeatable oval tracks and regular roads

1.4 Thesis Outline

This thesis consists of 8 chapters. Chapter 1 has introduced the work and provided the motivation for estimating the relative motion between the cabin and chassis. Chapter 2 will provide technical background for understanding the additional chapters by outlining the important navigation frames used within the work and introduce the base estimation technique, the Kalman filter, which other techniques will build upon. Chapter 3 describes the physical setup and location for collecting the data that will be used in validating the different techniques. Chapter 4 discusses the first method used to solve for the relative motion between the two bodies by using a normal GPS/INS integration but with noncolocated sensors. Chapter 5 will change the filter to a transfer alignment integration by adding states to compensate for the misalignment between the cabin and chassis. Chapter 6 analyzes potential improvements to the transfer alignment integration described in Chapter 5 and provides the results of the added improvements. Chapter 7 reduces the filter from Chapter 6 to make up for observability issues from the dynamic transfer alignment method. Finally, Chapter 8 provides the conclusions of this thesis and potential avenues for future work.

Chapter 2

Technical Background

This chapter provides the basis for both interpreting the results within this thesis and understanding methods that will later build upon the Kalman filter. The chapter will define all the different reference frames used within this thesis and the different ways that a user could both represent and transform attitude and orientation. As well as review how inertial measurements such as acceleration and angular rates can be used to determine a users position, velocity, and attitude. Additionally, this chapter goes over models that help to remove gravitational effects from inertial measurements. Finally, this chapter considers the estimation technique, the Kalman filter and will also provide a review of both the linear and a nonlinear version of the Kalman filter.

2.1 Coordinate Frames/Transformations

2.1.1 Earth-Centered Earth-Fixed Frame

The Earth-Centered Earth-Fixed (ECEF) Frame represents the 3-axis Cartesian coordinate frame that gives the user information about the location of an object on the Earth. The frames origin rests in the center of mass of the Earth. The Z-axis travels through the North and South Poles with positive values in the northern direction. Both the X and Y axis lie within the plane of the equator. The X-axis's positive direction goes through the prime meridian while the Y-axis's positive direction goes through the 90 degree east longitude. The geodetic reference

ellipsoid used for this thesis is the World Geodetic System 1984 (WGS84). Most of algorithms used in this thesis will use the ECEF frame and will be later converted to help convey information to the reader.

2.1.2 Local Navigation Frame

The local navigation frame has a fixed origin on the surface of the Earth and is usually a tangent plane to the geodetic reference ellipsoid. Popular variations of the local navigation frame are North-East-Down (NED) and East-North-Up (ENU) which both follow the right-handed orthogonal Cartesian system. These frames are common because it is much easier conceptually for a user to understand compared to an ECEF representation. This work uses the NED representation as the reference frame for the cabin and chassis body frames.

2.1.3 Body Frame

A body frame refers to a frame attached to a body within a local navigation or global frame. The bodies of interest in this thesis are the cabin and chassis frames. Both the cabin and chassis frames follow a similar convention that the X-axis is out of the front of the vehicle. The Y-axis is out the right-side of the vehicle and the Z-axis is pointed downward towards the road.

2.1.4 Sensor Frame

A sensor frame refers to a frame attached to a sensor that is mounted on an object of interest. There is often a misalignment during mounting between the body frame and a sensor frame such that an initial transformation between the two frames is required to ensure that sensors like IMUs are reflecting the body frame information instead of the sensor frame.

2.1.5 Euler Angles

This thesis uses Euler angles to represent the attitude of a body frame with respect to a reference frame. A roll angle will represent the rotation around the X axis, a pitch angle will represent the rotation around the Y axis and the yaw angle will represent the rotation around the Z-axis. The angles ϕ, θ, ψ will be used to reference roll, pitch, and yaw, respectively.

2.1.6 Direction Cosine Matrices

Direction Cosine Matrices (DCM) help to transform measurements between existing frames. This also means that they can be used to represent an object's attitude within a frame. This thesis will use the convention of R representing a rotation between 2 frames. The lower term of R will represent the current frame and the upper term will represent the frame the current frame exists within. For example, the term R_b^e represents the rotation matrix that would be used to convert measurements from the body frame into the ECEF frame. (e, n, b, cab, $chassis$, s) represent ECEF, NED, Body, Cab, Chassis, and Sensor frames.

A DCM can be made of three separate rotations around each axis using the matrices shown below.

$$R_x = \begin{bmatrix} 1 & 0 & 0 \\ 0 & cos(\phi) & sin(\phi) \\ 0 & -sin(\phi) & cos(\phi) \end{bmatrix} \tag{2.1}$$

$$R_y = \begin{bmatrix} cos(\theta) & 0 & -sin(\theta) \\ 0 & 1 & 0 \\ sin(\theta) & 0 & cos(\theta) \end{bmatrix} \tag{2.2}$$

$$R_z = \begin{bmatrix} cos(\psi) & sin(\psi) & 0 \\ -sin(\psi) & cos(\psi) & 0 \\ 0 & 0 & 1 \end{bmatrix}. \tag{2.3}$$

. These rotations can represent the rotation between the body frame and the navigation frame if multiplied together by applying Equations (2.4 - 2.5).

$$R_n^b = R_x R_y R_z \tag{2.4}$$

$$R_b^n = R_n^{b\,T}. \tag{2.5}$$

A rotation from the NED frame to the ECEF frame would follow a similar process and use a reference Latitude and Longitude (L,λ).

$$R_n^e = \begin{bmatrix} -sin(L)cos(\lambda) & -sin(\lambda) & -cos(L)cos(\lambda) \\ -sin(L)sin(\lambda) & cos(\lambda) & -cos(L)sin(\lambda) \\ cos(L) & 0 & -sin(L) \end{bmatrix}, \tag{2.6}$$

This rotation matrix is found by multiplying two of the previous rotation matrices from Equations (2.1 - 2.3) and using the Latitude and Longitude angles and the result is given in Equation (2.6). The rotation in Equation (2.6) can be used in conjunction with the rotation in Equation (2.5) to determine the rotation between body and ECEF, given below.

$$R_b^e = R_n^e R_b^n. \tag{2.7}$$

2.2 Inertial Mechanization

Inertial mechanization describes how inertial measurements are used to propagate the pose of an object. An IMU (inertial measurement unit) provides acceleration and angular velocity information at high update rates. However, most systems need to keep track of the position, velocity, and attitude of the sensor body. The inertial measurements are converted to position, velocity and attitude using 3 mechanization steps: Attitude Update, Acceleration Rotation, and the Position and Velocity Update. This thesis represents the attitude of the body using a DCM to transform the body measurements into the navigation frame. The position and velocity are kept in a vector that has x, y, and z components of the ECEF frame.

The DCM representing the attitude is propagated forward in time by using the angular rate inertial measurements. The angular rate measurements exist in the body frame and represent a change in attitude. To properly propagate the DCM, the angular rate measurements need to be converted from a vector of (ϕ, θ, ψ) components into its own DCM. This can be accomplished by first changing the angular rate vector into a skew-symmetric matrix.

A 3x3 skew-symmetric matrix can be used to represent cross products as matrix multiplications. Given $a = (a_1, a_2, a_3)$, a skew-symmetric form of that vector is given below.

$$[a]_x = \begin{bmatrix} 0 & -a_3 & a_2 \\ a_3 & 0 & -a_1 \\ -a_2 & a_1 & 0 \end{bmatrix}. \tag{2.8}$$

The skew-symmetric form of a vector will be represented by $[]_x$ when displaying a vector that is a collection of additional variables. Otherwise, the skew-symmetric form of vector will also be represented by a Ω symbol. A change in DCM can be calculated by multiplying the change in Euler angle in a skew-symmetric form and the current prediction of an objects attitude. This is shown in Equation (2.9).

$$\dot{R}_b^e = R_b^e \Omega_b \tag{2.9}$$

$\dot{R}_b^e$ can then be integrated using the 1st order Eulers method as shown below.

$$R_b^e(t + \Delta t) = R_b^e(t) + \dot{R}_b^e \Delta t - \Omega_e R_b^e. \tag{2.10}$$

The Ω_e term represents the angular rate of the Earth and Δt represents the change in time. Once the new DCM has been updated the user can rotate the acceleration measurements into the navigation frame from the body frame and remove external measurements such as gravitational effects (γ) using Equation (2.11).

$$f_e = R_b^e f_b - 2\Omega_e v_e + \gamma. \tag{2.11}$$

The term f_b represents the specific force measured by the IMU in the body frame and v_e represents the current velocity in the ECEF frame. Now the acceleration can simply be integrated to solve for velocity and position using Equations (2.12 - 2.13).

$$p_e(t + \Delta t) = p_e(t) + v_e(t)\Delta t + \frac{1}{2} f_e \Delta t^2, \tag{2.12}$$

$$v_e(t + \Delta t) = v_e(t) + f_e \Delta t. \tag{2.13}$$

2.3 Gravity Terms

In the previous section, the inertial mechanization required the removal of the gravitational effects because the IMU measures the combination of actual motion and gravity. Integrating this gravity term to find position and velocity would make an object appear as if it were in free fall even though the IMU remains static. When correcting the accelerometer in the ECEF frame there are a few terms that are important to consider: specific force, gravitational acceleration, and centrifugal acceleration. Specific force refers to what is sensed by the sensor, which can include the actual motion of the sensor body as well as acceleration due to gravity and rotation of the Earth. Gravitational acceleration is specific to what is sensed by the sensor in regards to the mass of the Earth. Lastly, centrifugal acceleration is acceleration due to the rotation of the earth. Gravity includes only the combination of the gravitational acceleration and the centrifugal acceleration and is the term that needs to be removed from the specific force to ensure that only the motion of the sensor is mechanized.

This thesis uses the World Geodetic System 1984 (WGS84) for the ellipsoid model of the Earth which was developed by the National Geospatial-Intelligence Agency (NGA). WGS84 was initially for military purposes but is now widely used by GPS and INS systems around the world making it a global standard for navigation systems. The parameters used in this model are displayed in Table 2.1 and a visual is provided by Figure 2.1.

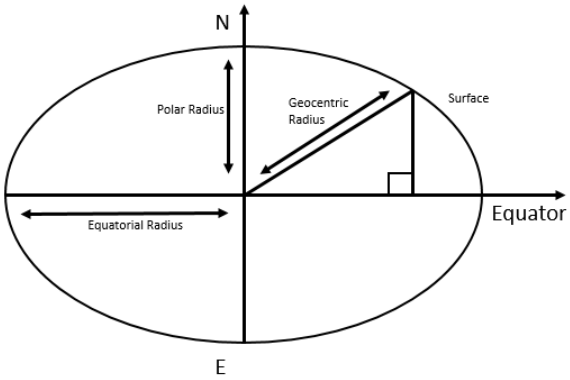

Figure 2.1: WGS84 Ellipsoid representation of the Earth

Gravitational acceleration can be calculated by using known information about the ellipsoid model of the Earth and the given position p_e of the sensor using Equation (2.14).

Table 2.1: WGS84 Parameters.

Parameter	Abbreviation	Value	Units
Earths 2nd Gravitational Constant	J_2	$1.082627e-3$	Constant
Earths 1st Gravitational Constant	μ	$3.986004418e14$	$\frac{m^3}{s^2}$
Earths Rotation Rate	ω_e	$\begin{bmatrix} 0 \\ 0 \\ 7.2921159\text{e-}5 \end{bmatrix}$	$\frac{rad}{s}$
Equatorial Radius	R_o	6378137	m
Polar Radius	R_p	6356752.31425	$\frac{rad}{s}$
Flattening	f	298.257223563^{-1}	Constant
Eccentricity	ec	0.0818191908425	Constant

$$\gamma = \frac{-\mu}{\|p_e\|^3}\left\{p_e + \frac{3}{2}J_2\frac{R_o^2}{\|p_e\|^2}\left\{\begin{bmatrix}[1-5(\frac{p_e(1)}{\|p_e\|})^2]p_e(1) \\ [1-5(\frac{p_e(2)}{\|p_e\|})^2]p_e(2) \\ [3-5(\frac{p_e(3)}{\|p_e\|})^2]p_e(3)\end{bmatrix}\right\}\right\}. \tag{2.14}$$

Gravity can then be calculated by including the rotation rate of the Earth and the gravitational acceleration as shown below.

$$G_e = \gamma - \Omega_e\Omega_e p_e. \tag{2.15}$$

Later in this thesis, important terms related to the world model will be used when deriving the state transition model for the extended Kalman filter. The key terms are Transverse Radius R_e and Geocentric Radius R_g. They are calculated using Equations (2.16 - 2.17).

$$R_e = \frac{R_o}{\sqrt{1-ec^2 sin(L)sin(L)}}, \tag{2.16}$$

$$R_g = R_e\sqrt{cos(L)cos(L) + (1-ec^2)^2 sin(L)sin(L)}. \tag{2.17}$$

2.4 Kalman Filter

The main technique used to combine sensor measurements in this thesis is the Kalman filter. It provides an optimal way to combine current state (pos., vel., att.) information and incoming measurements. The Kalman filter is able to combine current sate information with incoming measurements by keeping a mean and variance of the estimates. It updates these estimates with the state transition model which propagates the state estimates in time in the absence of new measurements. Then when a measurement is received the Kalman filter will use the observation model to relate the new measurements with the current estimates. The Kalman filter, using both the state transition and observation models operates through a prediction and update procedure. The mean and variance can be used to construct Gaussian distributions that represent the confidence the filter has with the mean values of both the state estimates and the incoming measurements. The filter essentially combines these to determine an optimal state estimate. The Kalman filter procedure is demonstrated in Figure 2.2. Which shows the Gaussian curve created by the mean and variance of the current state estimates and how the incoming measurements can be compared to find new means and variances.

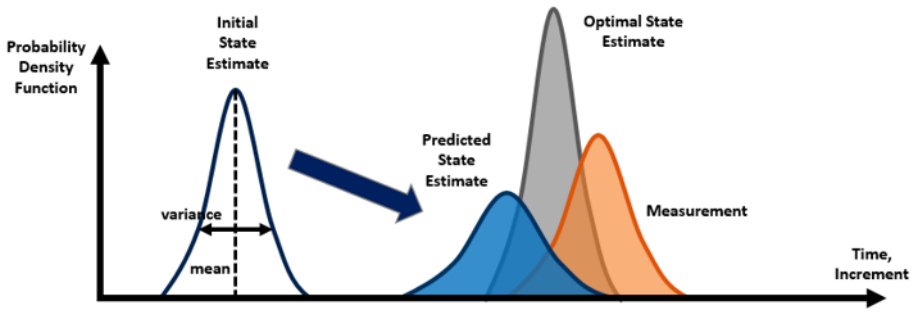

Figure 2.2: Kalman Filter Visual [4]

The prediction procedure propagates the estimate's mean and variance in the absence of new measurements using Equation (2.18 - 2.19).

$$\hat{x}_{k+1} = F\hat{x}_k + Bu_k + v_k \tag{2.18}$$

$$P_{k+1} = FP_kF^T + Q. \tag{2.19}$$

The state transition matrix is represented by the term F. It is used to model how state estimates are related to one another and how the state estimates and variances will change over time. $\hat{x}$ is the vector of state estimates, u is the inputs to the system, B represents how inputs effect the states, and v is a representation of the noise on the system. P and Q are the state covariances and the process noise, respectively.

The update procedure utilized the mean and variance of the measurement to combine the measurements with the current state estimate's to find an optimal solution by using the observation model H to relate the measurements and states using Equations (2.20 - 2.22).

$$K_k = \frac{P_kH^T}{HP_kH^T + R_{noise}} \tag{2.20}$$

$$y = z - H\hat{x_k} \tag{2.21}$$

$$\hat{x_{k+1}} = \hat{x_k} + Ky \tag{2.22}$$

$$P_{k+1} = (I - KH)P_k(I - KH)^T + KR_{noise}K^T \tag{2.23}$$

In the above equations, y represents the innovation or difference between the measurements and the current estimates. K is the Kalman gain which uses the current state covariances and the incoming measurements covariance to determine how much to scale the innovation to properly update the states.

2.4.1 Extended Kalman Filter

The main downside to a Kalman filter is that it assumes a linear state transition model and observation model. The linear assumption is due to the requirement that the mean and covariance need to be represented by a Gaussian curve for the Kalman filter solution to be optimal. Most real world systems are nonlinear in nature including the work explained in this thesis.

One alternative to the Kalman filter to account for non-linear systems is the is the extended Kalman filter. The extended Kalman filter linearizes the nonlinear state transition and observation models to be able to update the variance of the states. This helps to maintain the Gaussian representation of the mean and variance which is a fundamental assumption of the Kalman filter. A visual representing this linearization is shown in Figure 2.3.

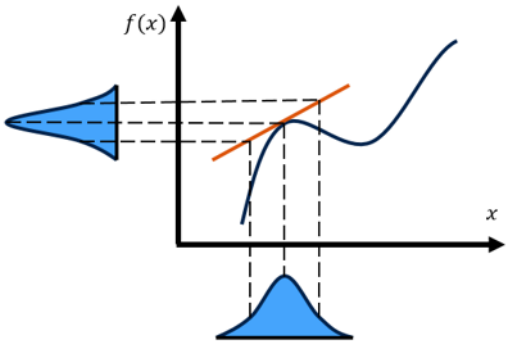

Figure 2.3: Extended Kalman Filter Visual [4]

The state transition model can be represented by a nonlinear function f that has inputs $\hat{x}$ and u. The state transition matrix that is used for updating the state covariance information is a linearized form of the state transition nonlinear function formed by taking a Jacobian of function shown in Equations (2.24 - 2.25).

$$\hat{x}_{k+1} = f(\hat{x_k}, u_k) + v_k \tag{2.24}$$

$$F = \left.\frac{\partial f}{\partial x}\right|_{\hat{x}_{k-1}, u_{k-1}}. \tag{2.25}$$

The observation model follows the same process as the state transition model. The innovation can be found using a nonlinear function h with $\hat{x}$ as an input and the observation matrix can be calculated by taking a Jacobian of that nonlinear function as shown in Equation (2.26 - 2.27).

$$y = z - h(\hat{x_k}) \tag{2.26}$$

$$H = \left.\frac{\partial h}{\partial x}\right|_{\hat{x}_{k-1}} . \tag{2.27}$$

The extended Kalman filter is one solution to the problem of non-linear state estimation. The EKF, however is not without its disadvantages. The linearization causes the filter to be very sensitive to initial conditions. Also, because the linearization is only an approximation of the state transition and observation models, the extended Kalman filter is not guaranteed to be an optimal solution like the linear Kalman filter.

This section concludes the technical background needed for this thesis. Chapter 3 follows this chapter with the test setup and evaluation methods that will be used to evaluate and understand the results in future chapters.

Chapter 3

Experimental Test Setup and Evaluation

This chapter will review the experimental setup used for data collection including descriptions of both the quality of sensors used for estimation as well as truth systems used to analyze the performance of the proposed algorithms. Specifically, this chapter discusses the different truth sources and their relevance to the work. The test locations where data was collected are described and distinct features between the different locations will be highlighted.

3.1 Test Setup

The vehicle used in this thesis is a Peterbilt 579 semi-truck. The cabin of the truck is outfitted with a Novatel FlexPak6D that provides GPS measurements and a Memsense 3020 that provides the inertial measurements. The GPS/INS system used for truth on the cab is the Honeywell eTALIN 5000. A XSENS MTi 300 provides the chassis inertial measurements and the chassis also uses a Honeywell eTALIN 5000 for truth measurements. The cabin eTALIN uses the same antenna as the Novatel GPS receiver. These tests were performed with no trailer to ensure that the GPS/INS system on the chassis could properly receive satellite signals. The truck and the hardware setup is shown in Figure 3.1 and all individual sensors are shown in Figure 3.2. The cabin GPS receiver antenna is located within the fairing but is still able to properly receive GPS signals.

All sensors are connected to the same Linux computer that is located within the truck cabin. The sensors were recorded using ROS (Robot Operating System) architecture. ROS is an open-source robotics middleware suite and itself is not an operating system (OS) but a set

(a) GAVLAB Peterbilt 579 Truck (b) Rear Setup

Figure 3.1: Truck Setup

of software frameworks for robot software development. ROS provides packages that allow for the recording of output messages from each sensor. Data was recorded by using appropriate ROS drivers for each of the sensors. The performance of each of the sensors used in these tests are shown in Tables 3.1, 3.2, and 3.3. These values are taken from each sensors respective datasheets that are available online.

(a) XSENS MTi 300 (b) Memsense 3020 (c) NovAtel FlexPak6D (d) eTALIN 5000

Figure 3.2: Sensors

Table 3.1: Inertial Measurement Units Performance

Sensor	Gyroscope		Accelerometer	
	Bias Instability	Noise Density	Bias Instability	Noise Density
XSENS MTi 300	10 deg/hr	0.01 deg/s/$\sqrt{Hz}$	15 μg	60 μg
Memsense 3020	1.06 deg/hr	0.06 deg/s/$\sqrt{Hz}$	14.8 μg	160 μg

A test run of two rigidly mounted eTALINs was performed to validate the truth measurements used in this thesis. Two rigidly mounted eTALINs represent a control case where the

Table 3.2: GPS Receiver Solution Performance

Sensor	Horizontal Position Accuracy	Velocity Accuracy
NovAtel FlexPak6D	Single Point L1-L2 1.2 m	0.03 m/s RMS

Table 3.3: eTALIN Solution Performance

Sensor	Heading Accuracy	Pitch/Roll Accuracy
Honeywell eTALIN 5000	<0.70 mils RMS	<0.35 mils RMS

standard deviation between the angle measurements can be used to represent the best performance the sensors can measure relative to each other. Since the eTALINS will be used to measure the relative motion of the cab and chassis, this test provides an estimate of the accuracy of the truth system. Figure 3.3a shows the dual eTALIN setup in the back of the GAVLABs Lincoln MKZ and Figure 3.3b shows the angle difference between both units from a dataset taken around the surrounding roads near Auburn University's NCAT test track (discussed in future section). The roll, pitch, and yaw angle differences had standard deviations of 0.0181, 0.0309, and 0.0234 degrees, respectively. The relative motion between the cabin and chassis bodies can be up to 1-2 degrees showing these sensors will provide relative accurate measurements compared to the motion being estimated.

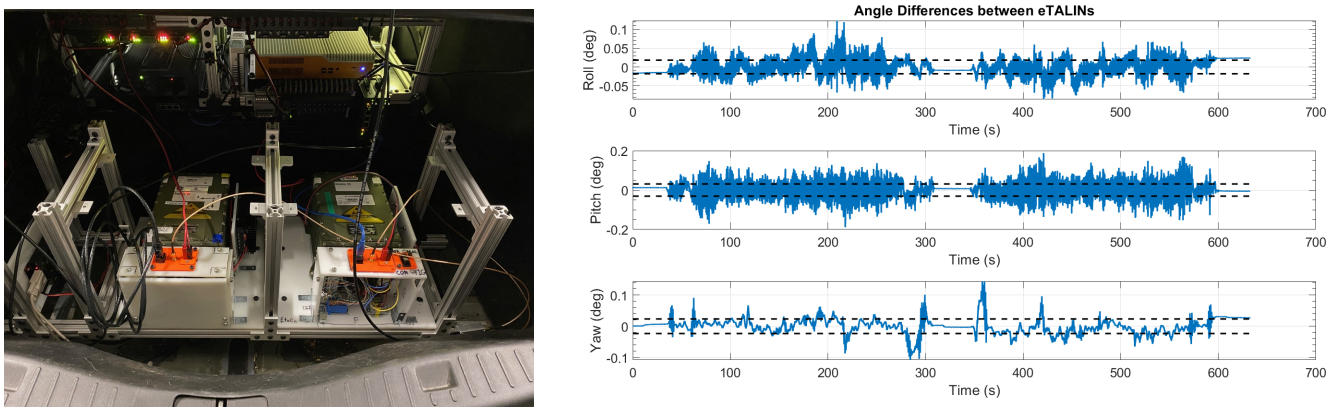

(a) Setup

(b) Results

Figure 3.3: eTALIN Comparison

3.2 Evaluation of Results

Results in this thesis will be evaluated by using 2 different set-ups and 2 different test locations. The first setup, will use measurements from the cabin eTALIN as a higher quality GPS/INS system in the filters created in later chapters. The second setup will use measurements from the lower quality Novatel and Memsense GPS/INS system. The two different test locations will be Auburn University's NCAT test track and roads surrounding the track. All estimators in this thesis will focus on estimating the chassis attitude and rely on the cabin sensors to act as a high quality master system. So, results will show the comparison between the chassis eTALIN attitude and the filters chassis attitude estimates.

3.3 Location

The tests were performed at the GAVLabs (GPS and Vehicle Dynamics Lab) Test Facility at the NCAT (National Center for Asphalt Technology) test track. The NCAT track is 1.7-mile oval with 2 lanes that mainly acts as an asphalt technology research facility but, the GAVLab also has access to it for autonomous navigation research. A birds eye view of the track is in Figure 3.4. Tests were also performed on Highway 280 and the surrounding roads. These routes will be referred to as the NCAT and Roads dataset, respectively.

Figure 3.4: National Center for Asphalt Technology in Auburn, AL

3.4 Dataset 1: NCAT Track

The NCAT track dataset includes 3 laps of the NCAT test track. The track is banked approximately 8 degrees on its west and east turns. The dataset is convenient for the analysis of the methods because it provides constant reoccurring situations where there is substantial difference between the cabin and chassis. Figures 3.5 and 3.6 highlight the difference in motion between the two bodies in both the velocity and attitude.

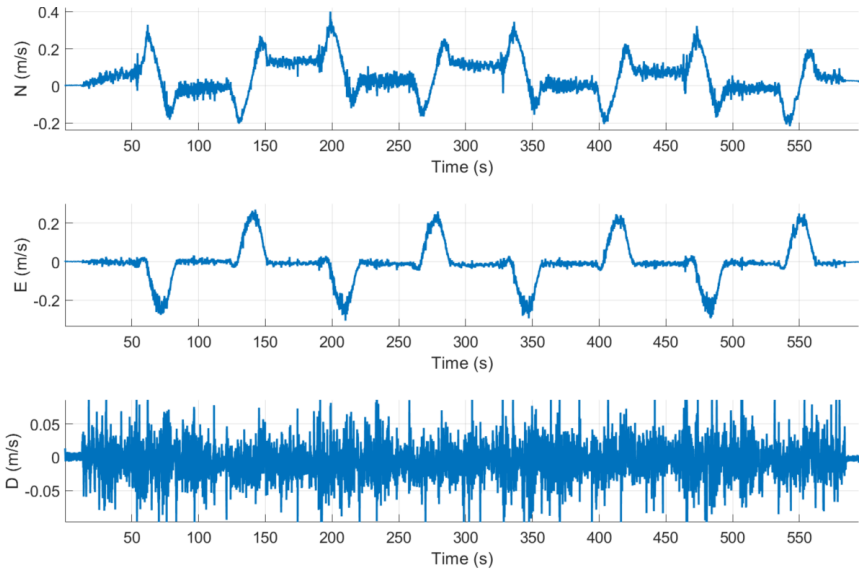

Figure 3.5: Relative NED Velocity (Cabin minus Chassis)

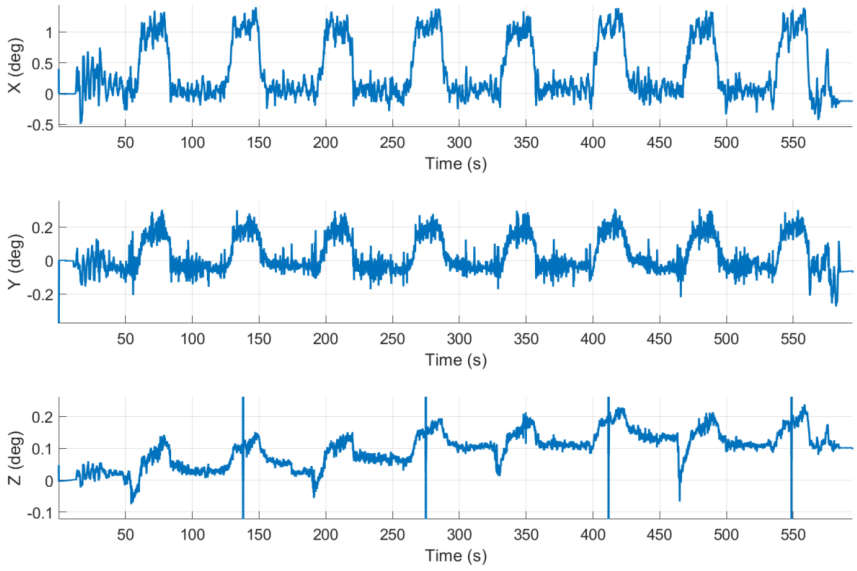

Figure 3.6: Relative Attitude (Cabin minus Chassis)

3.5 Dataset 2: Roads

The Roads dataset includes driving on the roads that are near the NCAT track facility. The path followed by the semi-truck is displayed in Figure 3.7. This dataset has larger elevation changes so there is a slight increase in the excitation in the pitch direction. However, most of the driving is along fairly straight roads removing a lot of excitation in the yaw direction.

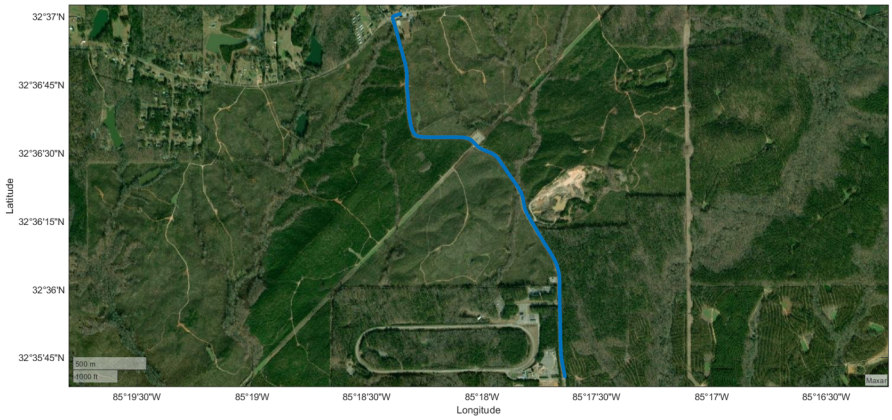

Figure 3.7: Roads Location

Figure 3.8 and 3.9 plot the relative attitude and relative velocity between the cabin and chassis for the Roads dataset. These plots shows that the largest difference in attitude still comes from the roll direction (approx. 2 deg) while the pitch and yaw directions remain mostly the same when comparing the cabin and chassis solutions. The goal of this thesis will to be focus on the roll and pitch directions because they are the largest relative angles that will effect perception sensors.

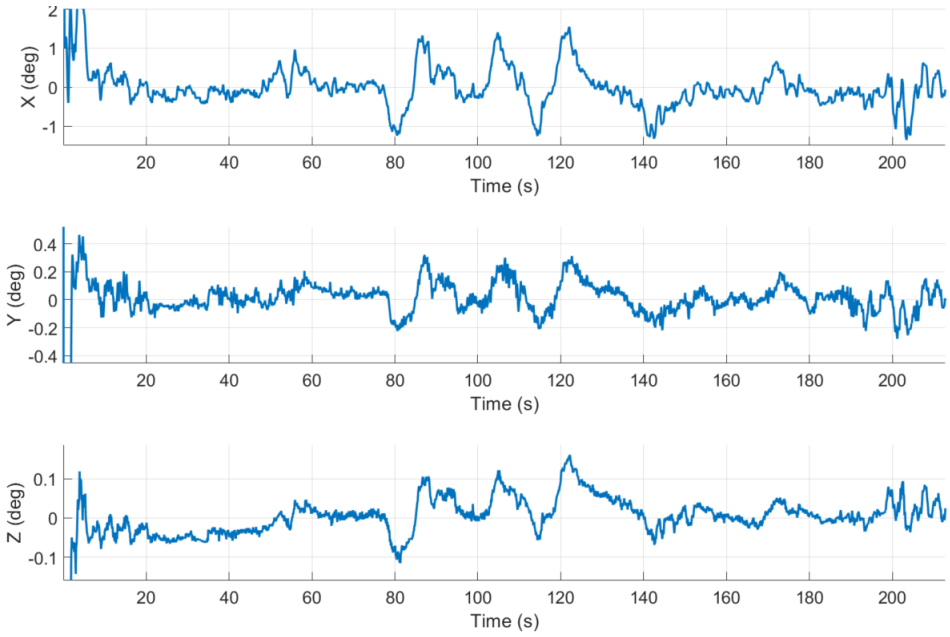

Figure 3.8: True Relative Attitude (Cabin - Chassis)

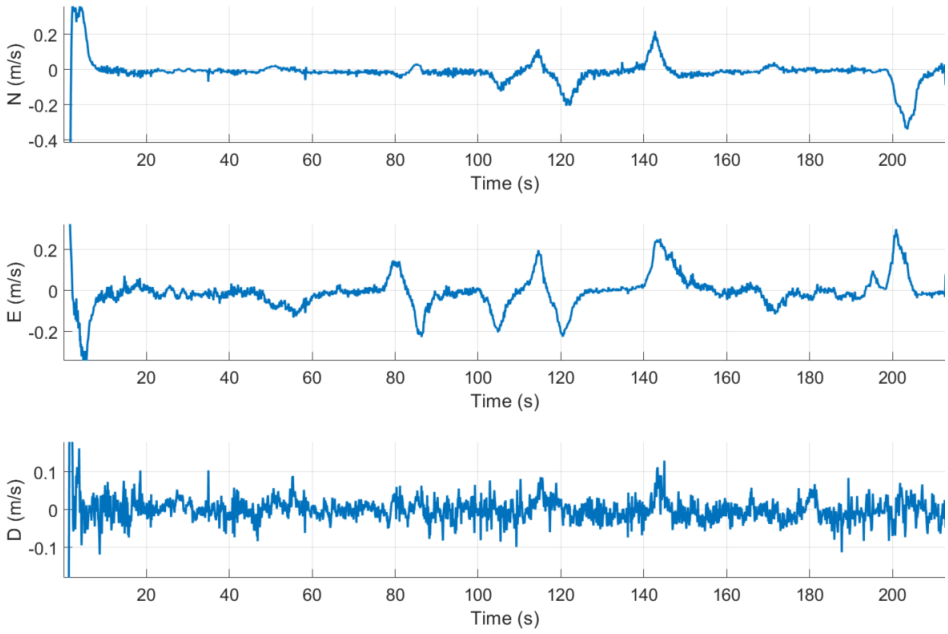

Figure 3.9: True Relative Velocity (Cabin - Chassis)

Chapter 4

Dual GPS/INS using One GPS Antenna

The GPS/INS method in this chapter uses the GPS antenna that is mounted on the cabin of the vehicle to help correct the cabin and chassis IMU errors. Once those errors are corrected the attitude and velocity information from the cab and chassis can be compared to determine the relative motion. This process for the GPS/INS cab-chassis motion estimation on the truck is depicted in a block diagram format in Figure 4.1. Note that this method uses the same GPS antenna (located on the cab roof) for both inertial sensors creating the need for two extended Kalman filters.

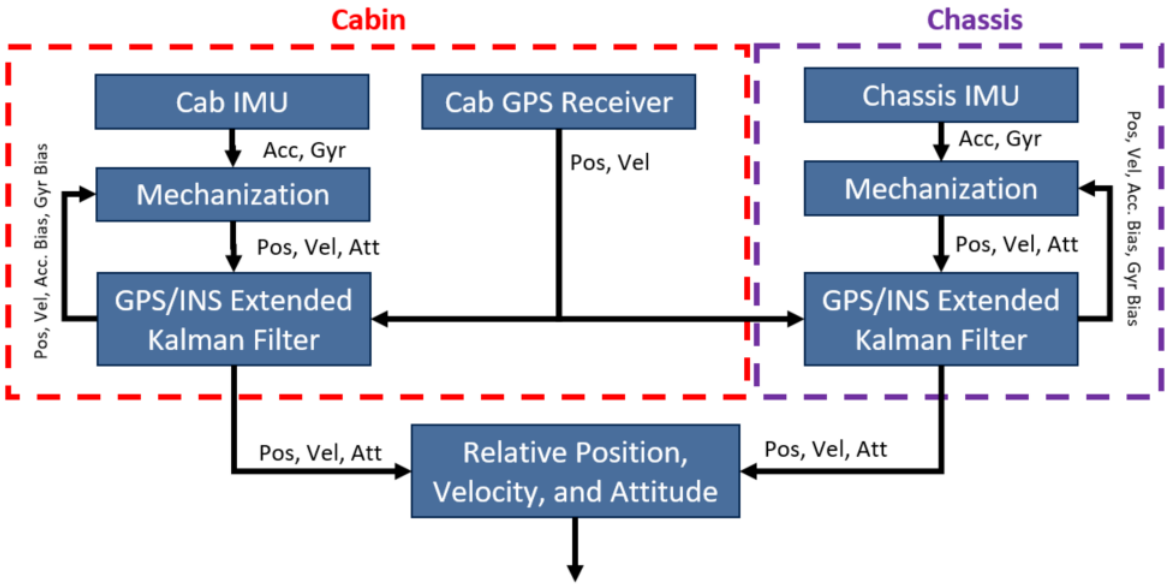

Figure 4.1: Dual GPS/INS Method Block Diagram

The GPS/INS method uses an error-state EKF for both the cabin and chassis IMUs. The states used in these filters are given below.

$$\hat{X} = \begin{bmatrix} \delta p_e \\ \delta v_e \\ \delta \Phi \\ b_a \\ b_g \end{bmatrix}. \tag{4.1}$$

The terms, δp_e, δv_e, $\delta \Phi$ represent the error in the position, velocity, and attitude. This filter uses error states instead of the true physical states due to the linearizing of the nonlinear equations. By using error-states the filter is always linearizing around the same equilibrium point (of zero) instead of that point changing through out the course of a dataset. This helps maintain the stability of the filter.

The bias terms, b_a and b_g represent the bias (or error) in the acceleration and gyroscope measurements, respectively. These biases represent the difference between a true and measured acceleration and angular rate as described below.

$$[f_b]_{meas} = [f_b]_{true} - b_a \tag{4.2}$$

$$[w_b]_{meas} = [w_b]_{true} - b_g. \tag{4.3}$$

4.1 Prediction Update

Previous sections presented the inertial mechanization formula as a full state formula. However, this chapter will now utilize an error state version of that mechanization. The error state version is derived by taking a difference between a true and estimated position, velocity and attitude equations. The error states can be found by using the Equations (2.11 - 2.12) and this derivation is detailed in [10]. Resulting error state equations from using the previous mechanization equations are given now in Equations (4.4 - 4.6).

$$\delta \dot{p_e} = \delta v_e \tag{4.4}$$

$$\delta \dot{v_e} = [-R_b^e f_b]_x \delta\Phi_e + R_b^e \delta f_b - 2\Omega_e \delta v_e + \frac{-2\gamma p_e^T}{R_g(L)\,\|p_e\|}\delta p_e \tag{4.5}$$

$$\delta\dot{\Phi}_e = -\Omega_e \delta\Phi_e + R_b^e \delta\omega_b \tag{4.6}$$

In the above equations, terms like δf_b and δw_b can be represented by the acceleration and angular rate bias terms b_a and b_g. Modelled using a 1st-Order Markov Process given in Equations (4.7 - 4.8). This bias model ultimately assumes that the acceleration and angular rate biases will be close to zero mean over a long enough time period. The Markov Process model also includes an additional parameter, correlation time, that represents how quickly the biases are expected to converge to that mean. A higher correlation time will take longer to converge compared to a lower value. The process is described with Equations (4.7) and (4.8).

$$\dot{b_a} = \frac{-1}{t_a} b_a \tag{4.7}$$

$$\dot{b_g} = \frac{-1}{t_g} b_g. \tag{4.8}$$

Note that t_a and t_g represent the correlation time for the biases. Now that the INS error model has been defined, the state transition matrix can be formulated by finding the Jacobian of the previous error state equations. The continuous and discrete forms of that Jacobian are represented by Equations (4.9) and (4.9).

$$\begin{bmatrix} \delta\dot{p_e} \\ \delta\dot{v_e} \\ \delta\dot{\Phi}_e \\ b_a \\ b_g \end{bmatrix} = \underbrace{\begin{bmatrix} 0 & I & 0 & 0 & 0 \\ \frac{-2\gamma p_e^T}{R_g(L)\|p_e\|} & -2\Omega_e & -[R_b^e f_b]_x & R_b^e & 0 \\ 0 & 0 & -\Omega_e & 0 & R_b^e \\ 0 & 0 & 0 & \frac{-1}{t_a} I & 0 \\ 0 & 0 & 0 & 0 & \frac{-1}{t_g} I \end{bmatrix}}_{F} \begin{bmatrix} \delta p_e \\ \delta v_e \\ \delta\Phi_e \\ b_a \\ b_g \end{bmatrix} \tag{4.9}$$

$$J = I_{[15x15]} + F\Delta t \tag{4.10}$$

The term I represents a 3x3 identity matrix and 0 represents a 3x3 zeros matrix. J represents the discrete form of the state transition matrix, using a Euler approximation to discritize the continuous state transition matrix.

Both the inertial mechanization and the error-state model can be simplified if the Earths rotation rate is removed. The Earths rotation rate can be removed when the magnitude of the noise floor of the inertial sensors is above the magnitude of the Earths rotation rate (1e-5 rad/s).

In the Section 2.4, Q is a model of noise or disturbance on a system. The noise from the IMU sensor was shown in Section 3.1 and can be related to the error states through the use of the process noise matrix,

$$Q = \begin{bmatrix} \sigma^2_{a_{w_N}} & 0 & 0 & 0 \\ 0 & \sigma^2_{g_{w_N}} & 0 & 0 \\ 0 & 0 & \sigma^2_{a_{w_B}} & 0 \\ 0 & 0 & 0 & \sigma^2_{a_{w_B}} \end{bmatrix}. \tag{4.11}$$

The terms, a and g represent accelerometer and gyroscope and the ω_N and ω_B represent the white noise and bias noise. The white noise represents noise on the final output from the inertial sensor while the bias noise represents a variance on the noise driving the change in the biases. Additional noise terms are ignored because their magnitude is insignificant compared to the bias and white noise terms.

The noise terms determined in Section 3.1 came from the sensor frame. To relate the sensor frame noise terms to the error-states a transformation matrix is used. Noise on the acceleration and angular rate terms have to be rotated into the ECEF frame for the position, velocity and attitude states. The biases noise terms can remain in the sensor frame. Taking this into account the transformation matrix for the noise terms can be formulated, resulting in Equation (4.12). The computation of the discrete version of the process noise matrix is shown in Equation (4.13).

$$B = \begin{bmatrix} 0 & 0 & 0 & 0 \\ R_b^e & 0 & 0 & 0 \\ 0 & R_b^e & 0 & 0 \\ 0 & 0 & I & 0 \\ 0 & 0 & 0 & I \end{bmatrix} \tag{4.12}$$

$$Q_d = BQB^T \Delta t \tag{4.13}$$

Once the state transition matrix, J, and the process noise matrix, Qd, have been derived the state covariance matrix, P, can be updated using Equation (2.19), given previously.

4.2 Measurement Update

The GPS/INS filter updates the cabin and chassis IMUs with GPS measurements from the cabin antenna. In a loosely-coupled filter the measurements used are only the final position and velocity calculated by the GPS receiver in the ECEF frame. This makes the relationship between the measurement and the filter states quite trivial because they are directly comparable.

An error measurement can be calculated by taking the difference between the GPS measurement and the current state estimates displayed below.

$$z = \begin{bmatrix} [p_e]_{GPS} - \hat{p_e} \\ [v_e]_{GPS} - \hat{v_e} \end{bmatrix} \tag{4.14}$$

These measurements can be directly related to the error-states through a linear observation model shown in Equation (4.15).

$$H = \begin{bmatrix} I & 0 & 0 & 0 & 0 \\ 0 & I & 0 & 0 & 0 \end{bmatrix} \tag{4.15}$$

However, the equations assume that the antenna is located at the same location as the IMU. The introduction of a lever arm adds more complexity to the linear observation model because the errors in the attitude estimates will now effect the difference between the GPS measurement

and the estimates of position and velocity. The observation model must be augmented to include the lever arm. The new measurement and observation model are shown below in Equations (4.16 - 4.17).

$$z = \begin{bmatrix} (p_{eGPS} - R_b^e l_b) - \hat{p_e} \\ (v_{eGPS} - R_b^e \Omega_b l_b + \Omega_e R_b^e l_b) - \hat{v_e} \end{bmatrix} \tag{4.16}$$

$$H = \begin{bmatrix} I & 0 & -[R_b^e l_b]_x & 0 & 0 \\ 0 & I & -[R_b^e \Omega_b l_b - \Omega_e R_b^e l_b]_x & 0 & -R_b^e [l_b]_x \end{bmatrix} \tag{4.17}$$

Once the measurement and observation model have been defined the GPS update can proceed using Equations (2.20 - 2.23) given previously.

4.3 Correction

The error-state EKF has one additional step to correct the physical states with the determined error states. After correcting the physical states the error-states are set to zero since that error has been removed from the physical state estimates as shown in Equations (4.18 - 4.20).

$$\hat{p_e} = \hat{p_e} + \delta\hat{p_e} \tag{4.18}$$

$$\hat{v_e} = \hat{v_e} + \delta\hat{v_e} \tag{4.19}$$

$$R_b^e = \frac{2I + [\delta\hat{\Phi}]_x}{2I - [\delta\hat{\Phi}]_x} R_b^e \tag{4.20}$$

As seen above, the attitude correction is done using a rotation matrix. The errors in the attitude angles act as a change in angle similar to the angular rates used from the gyroscope. The bias terms for the accelerometer and the gyroscope are set directly from the error-states because the bias is an error between the measured and true inertial measurements such that they are not reset to zero.

4.4 Results

This section provides the initial results from the Dual GPS/INS method applied to the NCAT Dataset described in Chapter 3. The results are analyzed by determining the accuracy of the chassis attitude estimates compared to the truth (chassis eTALIN).

Figure 4.2 shows the attitude estimates from the chassis using the dual GPS/INS method labelled as GPS Only Filter compared to the truth senor used for this test labelled as Chassis eTALIN. The attitude comparison figure highlights the filters ability to track the chassis eTALINs truth system with only around 5-10 degrees of error. However, an observation can be made, that during periods where the vehicle is turning, there are differences between the eTALIN and dual GPS/INS methods solutions. These errors are especially apparent in the pitch comparison where the Dual GPS/INS solution is spiking to around -2 degrees during each turn of the NCAT track.

It is safe to assume that these errors are from the non-colocation of the GPS antenna and the chassis IMU. Recall that the filter introduced in this chapter assumes the GPS antenna, where the filter receives measurements, is rigidly mounted to the IMU that is being corrected on the chassis. However, as discussed previously there is relative differences in both the roll and pitch angles between the cabin and chassis bodies during the turns of the NCAT track.

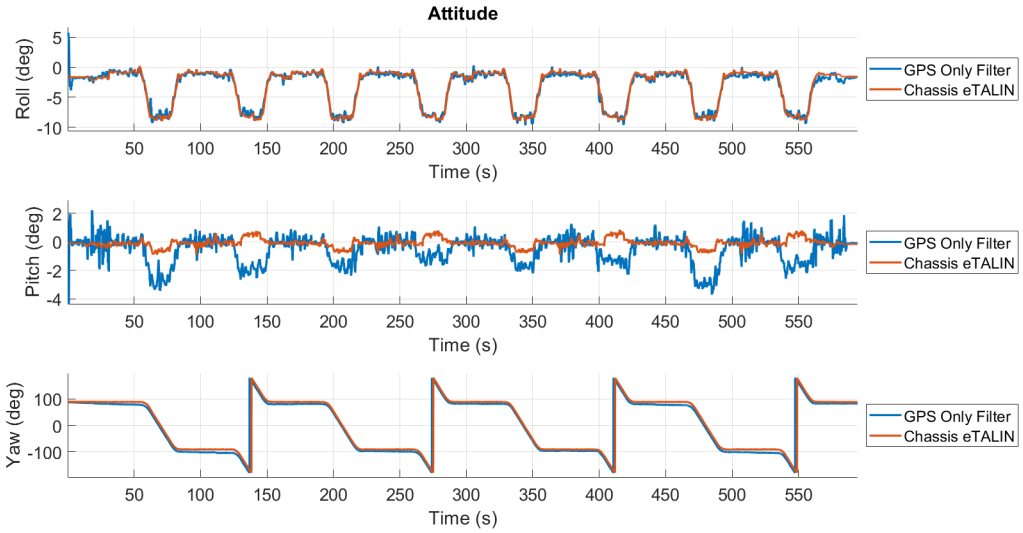

Figure 4.2: Comparison between Dual GPS/INS Chassis Attitude and Chassis eTALIN Attitude

Figure 4.3 provides the difference between the angles of the GPS/INS solution on the chassis and the chassis truth system. Additionally, Figure 4.3 further highlights another error that occurs using the Dual GPS/INS method. The error in the yaw angle can be seen to exhibit much larger drifts throughout the entirety of the dataset. The discontinuities originate from not unwrapping the yaw estimates. Therefore, these discontinuities don't represent spikes in the filter or truth solutions. This large drift most likely arises from a lack of observability for the yaw error state. This is specifically a deterministic observability problem. The loosely-coupled extend Kalman filter has been known to lack observability specifically for the yaw angle when there is not enough excitation.

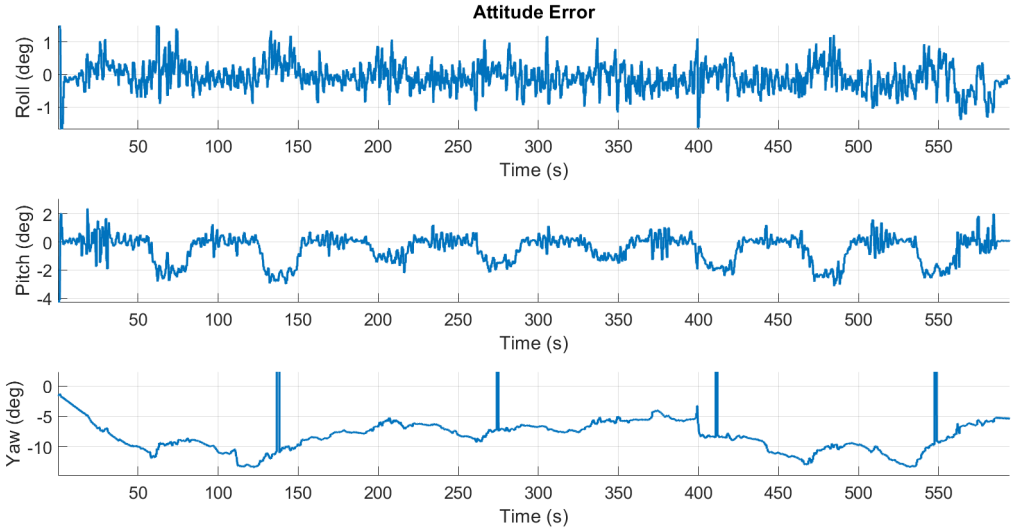

Figure 4.3: Error between GPS/INS Solution and Chassis eTALIN

Deterministic observability, which refers to the amount of motion the bodies need to experience to properly estimate the desired states. As outline earlier this filter uses position and velocity measurements in the update procedure to help correct not only position and velocity but also attitude and inertial biases. This is done through the state transition matrix that relates the position and velocity measurements to the other states that are being estimated. The velocity is related to the attitude through the acceleration of the chassis body as given previously in Equation (4.9). Figure 4.4 highlights this relation between the velocity error states and the attitude error states defined in the state transition matrix.

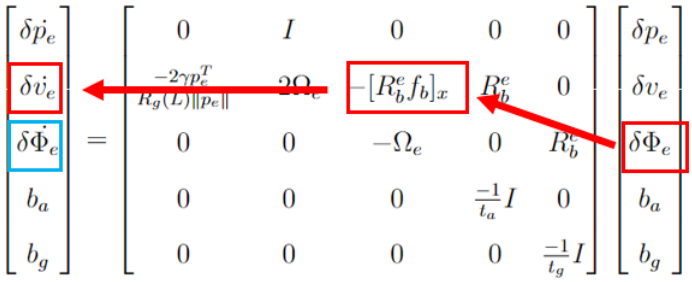

Figure 4.4: Relationship between Velocity and Attitude Error States

To fully observe all the attitude states properly there needs to be variation in the acceleration in the longitudinal, lateral, and vertical directions. However, the NCAT test track having only straight line and constant radius turn sections does not provide enough excitation to achieve this as seen in Figure 4.5. The yaw attitude error is affected by a lack of excitation of the acceleration in the lateral and longitudinal directions. The bulk of track dataset keeps a constant speed so there is already a lack of excitation in the longitudinal direction. During straight line driving there is zero lateral acceleration and during a constant radius turn at a constant speed there is only a constant lateral acceleration which still does not provide the needed excitation to estimate the yaw error state causing the large drifts in the yaw error.

Figure 4.5: NCAT Track highlighting Observability Challenges

Using the cabin GPS to correct the chassis IMU to estimate the relative error between the two bodies has challenges that are difficult to overcome. Therefore, this thesis will develop alternative methods that would use the combined solution from the cabin to be able to directly correct the attitude on the chassis in the following chapter. The method also does not require the rigid assumption between the two bodies that the GPS/INS method does. These changes should help to eliminate the large errors that are seen in the pitch and roll directions during the banked turns while also prevent the large drifts from the lack of observability.

Chapter 5

Transfer Alignment

In this chapter, the Dual GPS/INS method will be expanded by adding the attitude of the cabin as a measurement. Moreover, the new method does not assume that the two bodies are rigid to one another, but instead estimates a misalignment between them. This methodology is typically referred to as Transfer Alignment (TA). A block diagram including these additions is presented in Figure 5.1.

In the previous chapter, the assumption of the two bodies being rigid caused increased error during turns of the track. This occurred because there was relative motion between the two bodies. Now, by estimating the misalignment between bodies and applying an attitude measurement update, these errors should be removed. These changes will affect the state transition and observation models. The new method will add three states representing the misalignment angles in the three axis's between the cabin and chassis bodies. A user may add additional misalignment states related to the rate of change in the misalignment. However, because semi-trucks do not experience much excitation, it would be difficult to observe and separate out static and dynamic motion. Therefore, this addition is not applicable to the current work.

The state vector for the EKF with the transfer alignment method is updated below in Equation (5.1) which nowa include the additional misalignment states for each axis, represented by the symbol M.

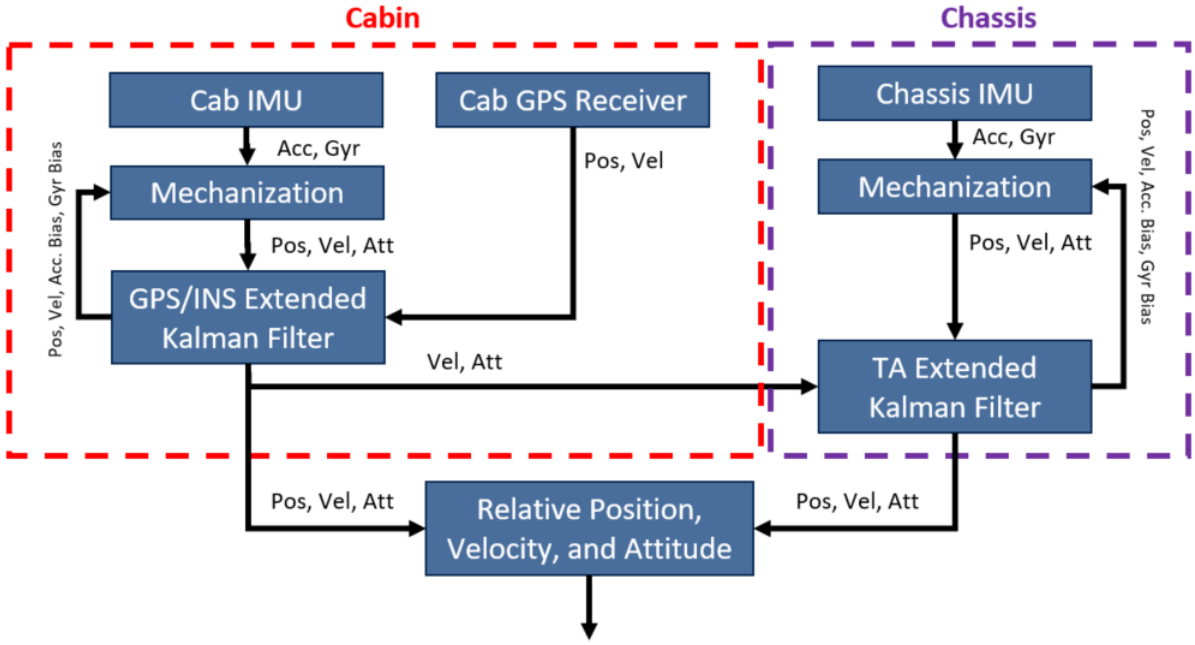

Figure 5.1: Transfer Alignment Method Block Diagram

$$\hat{X} = \begin{bmatrix} \delta p_e \\ \delta v_e \\ \delta \Phi \\ b_a \\ b_g \\ M \end{bmatrix} \tag{5.1}$$

5.1 Prediction Update

In addition to the previous state transition model in Equation (4.9), a first order Markov model is used to predict the change in the misalignment angle states over time.

The first order Markov model is a common choice for bias terms in estimation, particularly for acceleration bias in IMUs [10]. It is generically represented as Equation (5.2).

$$\dot{x} = -\frac{1}{t_M} x \tag{5.2}$$

The estimated state decays exponentially to zero over time by rate t_M. By decaying to zero, it maintains the zero-mean characteristics, which obeys the assumptions of the Kalman filter and is also a common characteristic of accelerometer bias terms. Similarly, a truck's suspension aims for a zero mean misalignment angle. This prompted the design choice of modelling the misalignment as a first order Markov process as well. The t_M term is user-defined and this term may change between trucks or can also depend on the dynamics of the route.

Equation (5.3) shows the updated state transition matrix, where the bottom right of the matrix includes the prediction model for the misalignment angles.

$$\begin{bmatrix} 0 & I & 0 & 0 & 0 & 0 \\ \frac{-2\gamma p_e^T}{R_g(L)\|p_e\|} & -2\Omega_e & -[R_b^e f_b]_x & R_b^e & 0 & 0 \\ 0 & 0 & -\Omega_e & 0 & R_b^e & 0 \\ 0 & 0 & 0 & \frac{-1}{t_a} I & 0 & 0 \\ 0 & 0 & 0 & 0 & \frac{-1}{t_g} I & 0 \\ 0 & 0 & 0 & 0 & 0 & \frac{-1}{t_M} I \end{bmatrix}. \tag{5.3}$$

The addition of new states necessitates a modification to the previous process noise matrix, Q, as well. A fictitious noise term is included to represent the degradation of the current misalignment estimate over time. This term represents uncertainty, because the first order Markov model is not a perfect model for the change in misalignment alignment. Note that the noise term is also user-defined, and the optimal term may vary depending on the dynamics of the semi-truck. With the addition of the new states, the input matrix B, which rotates the process noise terms into the same frames as the estimates states, must also be modified. However, the new noise terms are already in the same frame as the misalignment states so the B matrix only needs to include an identity matrix to transform the process noise matrix. These changes to the process noise and input matrix are reflected in Equations (5.4 - 5.5).

$$Q = \begin{bmatrix} \sigma^2_{a_{w_N}} & 0 & 0 & 0 & 0 \\ 0 & \sigma^2_{g_{w_N}} & 0 & 0 & 0 \\ 0 & 0 & \sigma^2_{a_{w_B}} & 0 & 0 \\ 0 & 0 & 0 & \sigma^2_{a_{w_B}} & 0 \\ 0 & 0 & 0 & 0 & \sigma^2_m \end{bmatrix} \tag{5.4}$$

$$B = \begin{bmatrix} 0 & 0 & 0 & 0 & 0 \\ R^e_b & 0 & 0 & 0 & 0 \\ 0 & R^e_b & 0 & 0 & 0 \\ 0 & 0 & I & 0 & 0 \\ 0 & 0 & 0 & I & 0 \\ 0 & 0 & 0 & 0 & I \end{bmatrix} \tag{5.5}$$

5.2 Measurement Update

Transfer alignment, as stated before, expands on the Dual GPS/INS method by including the attitude information from the cabin as a measurement for the chassis attitude. This measurement comes from a GPS/INS system mounted on the cabin. With this new information, an expansion of the previous innovation Equation (4.14) and observation model (4.17) is required. These changes ensure that the new cabin attitude measurement is properly related to the chassis attitude and new misalignment states.

The new observation matrix is shown in Equation (5.6).

$$H = \begin{bmatrix} 0 & I & 0 & 0 & 0 & 0 \\ 0 & 0 & I & 0 & 0 & R^e_{Chassis} \end{bmatrix} \tag{5.6}$$

Like the original GPS/INS EKF, the matrix is linear, because measurements can be directly related to the error states. But now, attitude error is related to both the error in the attitude solution as well as the current misalignment between the two bodies.

While other measurements, such as velocity, can be easily incorporated into the EKF's innovation equations, the cabin attitude requires a more thoughtful approach. One must consider the rotation between the cabin and ECEF frame, as well as potential misalignment. If the cabin and chassis are aligned, their rotation matrices, when multiplied together, would create an identity matrix. Therefore, any deviation from an identity matrix represents the collective error in estimated chassis attitude and the misalignment between the cabin and chassis. The innovation can then be calculated using the different components of R_e^e with Equation (5.7). The updated innovation needs to be converted from the DCM form (R_e^e) to a vector form. This process is shown in Equation (5.8).

$$I + [\delta\Phi + M]_x = R_{Cab}^e R_e^{Chassis} \tag{5.7}$$

$$z_{attitude} = \begin{bmatrix} -\frac{R_{e(2,3)}^e + R_{e(3,2)}^e}{2} \\ -\frac{R_{e(1,3)}^e + R_{e(3,1)}^e}{2} \\ -\frac{R_{e(1,2)}^e + R_{e(2,1)}^e}{2} \end{bmatrix} \tag{5.8}$$

5.3 Transfer Alignment Parameters

For the prediction step of the Transfer Alignment Method, the state covariance matrix, P, must be initialized. Additionally, the IMU process noise matrix, Q, must be set. These values are shown in Table 5.1. P was arbitrarily set, while the values in Q are derived from the sensor datasheet information which was given previously in Chapter 3.

Table 5.1: Left: Initial Covariances, Right: Process Noise Parameters

Parameter	Value	Units
ECEF Position (1 α)	0.2	meters
ECEF Velocity (1 α)	0.1	meters/sec
Attitude (1 α)	0.05	radians
Accelerometer Bias (1 α)	0.05	m/s^2
Gyroscope Bias (1 α)	0.05	rad/s

Parameter	Value	Units
Acc. White Noise (1 α)	0.005	m/s^2
Gyr. White Noise (1 α)	0.05	rad/s
Gyr. (Yaw) White Noise (1 α)	0.01	rad/s
Acc. Bias White Noise (1 α)	4e-4	m/s^2
Gyr. Bias White Noise (1 α)	3e-5	rad/s

Table 5.2 lists the noise parameters involved in the measurement update of the Transfer Alignment method. The cabin eTALIN's solution is used as the incoming measurement for

the chassis. See Chapter 3, Section 1 regarding eTALIN sensor performance. However, these values were tuned from the original datasheet values to maximize performance for the NCAT dataset.

Table 5.2: Measurement Noise Parameters

Parameter	Value	Units
ECEF Velocity (1 α)	7e-3	m/s
Roll (1 α)	6e-4	radians
Pitch (1 α)	1.5e-3	radians
Yaw (1 α)	6e-3	radians

5.4 Results

In this section, the Transfer Alignment method is applied to the NCAT and Roads datasets. The transfer alignment method uses the attitude of the cabin as a measurement for the chassis states to counteract problems seen in the original Dual GPS/INS method where pitch and roll angle errors increased during turns of the NCAT track. This was related to the non-colocation of the GPS antenna and the chassis IMU, which was not accounted for in the previous state transition and observation models. Additional errors were shown in the yaw angle, which were attributed to a lack of observability. This section will determine whether these issues can be addressed using the transfer alignment method.

Figure 5.2 shows the comparison between the Transfer Alignment method (TA filter) chassis attitude solution and the chassis eTALIN solution for the NCAT dataset. It is easy to see that the new TA filter's estimates of the chassis attitude more closely follows the true attitude measured from the eTALIN mounted on chassis compared to the previous GPS/INS filter (Figure 4.2). This fact is most prevalent in the pitch and yaw angle estimates.

Figure 5.3 shows the error between the TA filter chassis attitude solution and truth (the chassis eTALIN solution) for the NCAT track. This figure highlights the accuracy of the TA filter solution. The yaw error stays below 0.2 degrees. The pitch and roll angles experience a periodic error, where the maximum absolute error of the roll and pitch angles are 1 degree

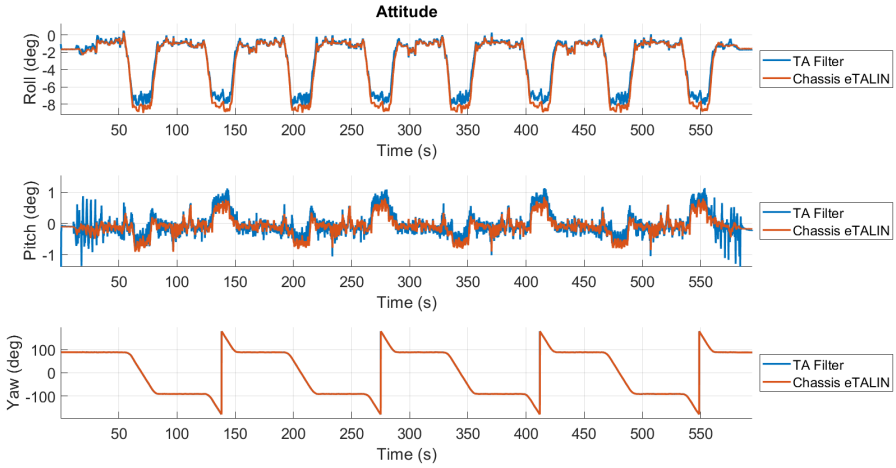

Figure 5.2: NCAT Attitude Transfer Alignment vs. Chassis eTALIN

and 0.4 degrees respectively. These results are very similar to the actual relative motion seen between the cabin and chassis for this dataset as shown previously in Figure 3.6.

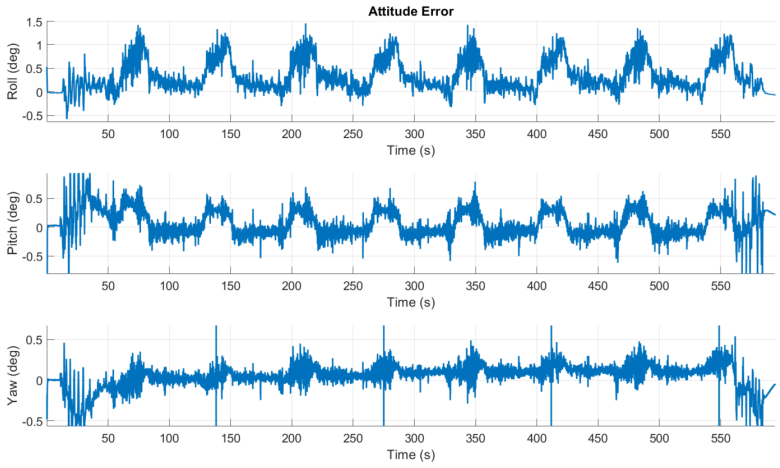

Figure 5.3: NCAT Attitude Error Transfer Alignment vs. Chassis eTALIN

Figure 5.4 presents the error between the TA filter chassis attitude and the "truth" for the Roads dataset. A similar trend, compared to the NCAT dataset, is found. The error is almost identical to the relative motion experienced by the semi-truck, as seen previously in Figure 3.8. The Roads dataset has higher error than the NCAT dataset, experiencing absolute roll error upwards of 1.2 degree and pitch and yaw absolute errors of around 0.3 degrees. Currently, these errors have similar magnitude to the actual relative motion.

Figures 5.5 - 5.6 shows the estimated misalignment angles for both the NCAT and Roads datasets. During turns, the estimated misalignment angles increase, as expected. However,

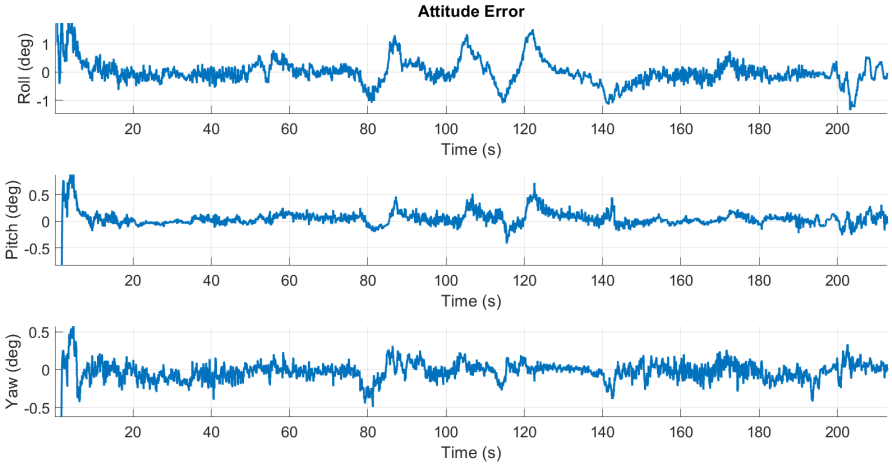

Figure 5.4: Roads Attitude Transfer Alignment vs. Chassis eTALIN

the estimation grows larger than the true misalignment angle values, which are typically 1-2 degrees maximum.

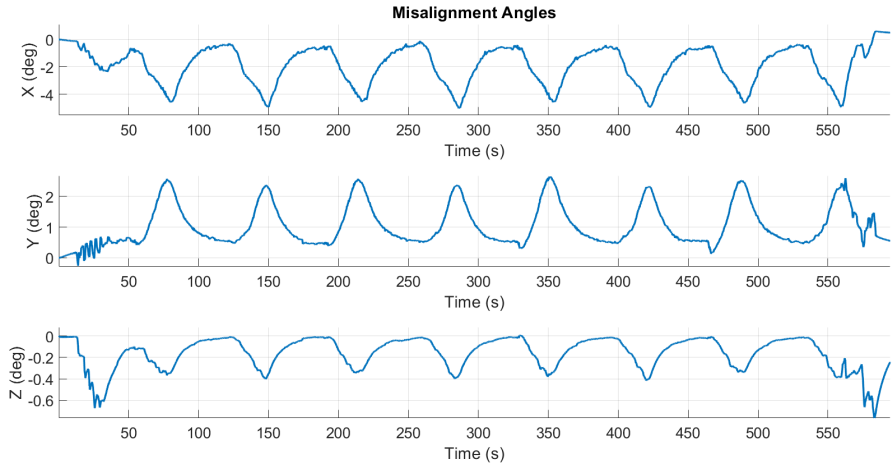

Figure 5.5: NCAT Dataset

5.5 Results Analysis

The original Dual GPS/INS EKF made the assumption that there was non-relative motion between the cabin and chassis, but this assumption led to failures (see Chapter 4). The error in the roll and pitch angles from Chapter 4 were attribute to the rigidity assumption, because increases in error only occurred during the banked turns of the NCAT track. This section of the NCAT test track is where there was the greatest amount of relative motion. Additionally, errors in the yaw angle were shown and were attributed to a lack of observability because of the dynamics

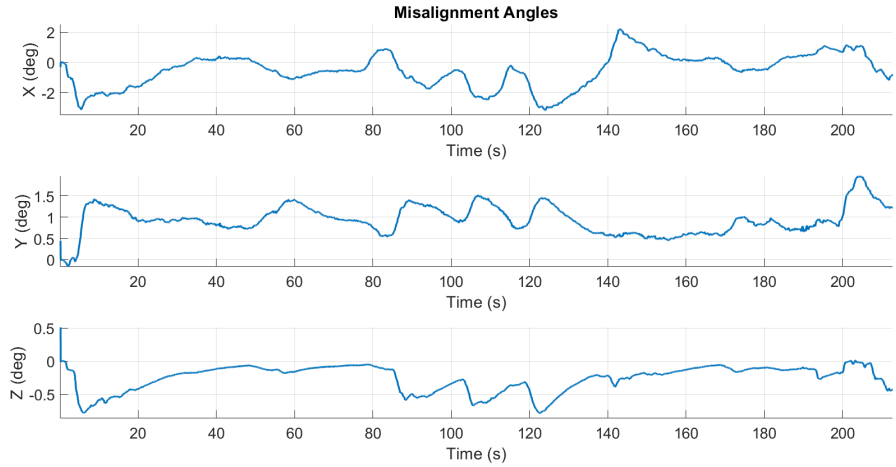

Figure 5.6: Roads Dataset

experienced. The NCAT track only has straight line driving and constant radius turns leading to the lack of excitation.

In this chapter, the TA filter added misalignment angle states and added the cabin attitude as a measurement in an attempt to mitigate these limitations. Overall, this effort was successful in addressing these errors, but it brought additional problems. The misalignment angles and the chassis attitude error highlight that the estimator has difficulty separating the misalignment angles and the chassis attitude from the cabin attitude solution's measurement. This is evident from the error attitude covariance results.

Figure 5.7 shows the attitude error covariance results for the NCAT track dataset. Two trends in the data are concerning: the saw-tooth pattern resulting from the measurement and the patterns in covariance with respect to locations of the NCAT track, specifically in the turns. The strong saw-tooth pattern calls attention to the fact that the incoming measurement is weighted heavily compared to the current estimate. This can cause the chassis attitude to overly match the cabin attitude measurement. While initially it could be assumed that the saw-tooth pattern is the result of tuning too favorably towards a measurement, it was found that any decrease in the confidence of the expected performance of the cabin solution largely decreased filter performance. As a result, the most successful filter currently overly matches the cabin attitude measurement.

Notice in Figure 5.7 and Figure 5.8 that the covariance shows specific trends at specific turns on the NCAT track. The change in the misalignment angles over time, as well as their relation to the incoming cabin attitude measurements, are not well modelled causing increases or decreases in the error attitude covariance during relative motion between the cabin and chassis bodies. This indicates that the first order Markov dynamic model for the misalignment angles may be overly simplistic.

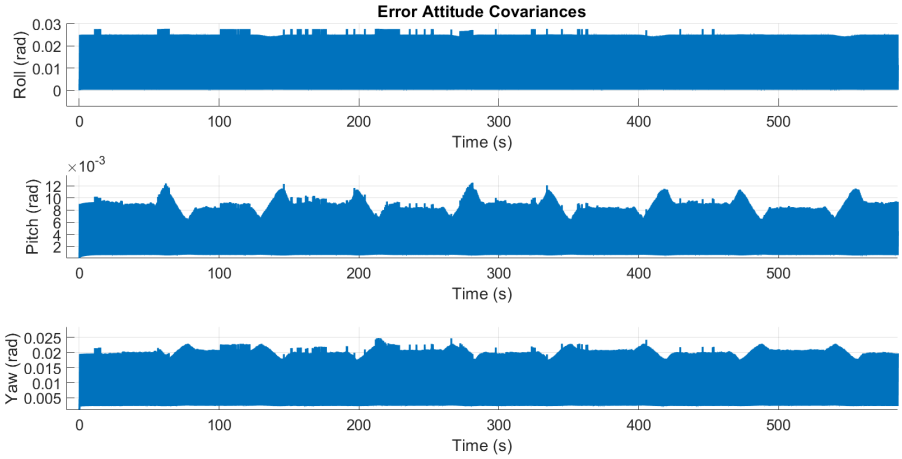

Figure 5.7: NCAT Attitude Covariance

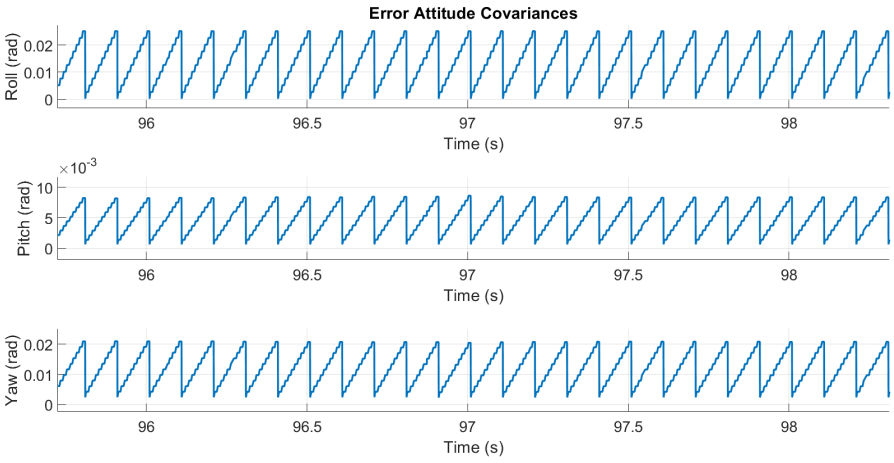

Figure 5.8: Zoomed-In NCAT Attitude Covariance

Having a poor model leads to an improper comparison between the current state and incoming measurement covariance. The Kalman filter assumes measurements follow a Gaussian distribution; if a measurement's mean and variance does not include the true value, then it would be considered a biased measurement. Biased measurements can lead to errors in the

Kalman filter. Unfortunately, the changes in covariance for specific turns in the NCAT track shows that there are biased measurements.

To improve the current Transfer Alignment solution, the current misalignment model must be improved. Furthermore, the only way to have confidence that a model has been improved is by introducing an analysis tool that can highlight potential biased measurements. Then, any method used to overcome the poor model of the misalignment angle can be verified. The next chapter addresses potential improvements to the TA filter to handle the biased measurements.

Chapter 6

Transfer Alignment Improvements

The prior chapter demonstrated that the Transfer Alignment improves the overall attitude estimation. It removes errors due to lack of observability and corrects the failings of the rigidity assumption from the original Dual GPS/INS method. However, creating a model that accurately defines the change in misalignment between the cabin and chassis is difficult. A poor state transition model can cause incoming cabin measurements to appear biased and create instability in the EKF.

In the previous chapter, it was also shown that the TA filter had issues with biased measurements because of a simplistic dynamic model for the misalignment angles. As the cabin becomes offset from the chassis, its attitude measurement will no longer meet the assumptions made by the Kalman filter unless the misalignment angles are modelled properly. Essentially, the cabin attitude becomes a non-zero mean measurement of the chassis attitude. If this measurement were to be used within the filter, it may cause stability issues and unwanted errors in the final attitude solution.

This chapter explores potential solutions to the poor misalignment state model. These solutions will come in a few different forms. First, a solution where the model is removed all together and only perform updates when there is no relative motion between the cabin and chassis is investigated. Other solutions that uses a more complex misalignment models, such as higher order Markov model or including additional states to assist the modelling are explored. Lastly, instead of modifying the state transition model, the simple solution of dynamically changing the measurement covariance to appear non-biased to the state estimates is evaluated.

A tool will be developed to determine when these methods appear biased to the state estimates and will be used as means to evaluating them.

6.1 Fault Detection

To evaluate the methods proposed in this chapter, there first needs to be way to quantize how well the model is performing for the Kalman filter. Fault detection is a method used to determine if incoming measurements fail the assumption of the Kalman filter. The Kalman filter assumes that an incoming measurement's mean and covariance are linearly related to the current filter states, because both are modelled as Gaussian distributions. Both Gaussian distributions are meant to contain the true value; so if either are biased, where the mean and variance are incorrect, then this will create instability that leads to errors in the final solution. The state transition model can cause the attitude states to be biased creating errors in the solution. This can become the case for the semi-truck if the misalignment angles are mis-modelled, because there is no longer a proper relationship between the cabin measurements and the chassis states.

Fault detection is able to detect these biased measurements by using the normalized innovation equation. The normalized innovation uses the current state's covariances and observation model, along with the incoming measurements and covariance, to determine if the incoming measurement can fit into the current state Gaussian. If not, the measurement is assumed to be biased. The normalized innovation is made up of Equations (6.1) and (6.2).

$$y = \frac{z - \hat{z}}{\sqrt{C}} \tag{6.1}$$

$$C = HPH^T + R \tag{6.2}$$

The variable y represents the normalized innovation. The user creates a threshold based on how much the normalized error is expected to overlap. This threshold is demonstrated in Figure 6.1.

Figure 6.2 shows the normalized innovation for both the attitude and velocity measurements over the course of the NCAT track. The normalized innovation in the current TA filter shows increased spikes during the banked turns (light blue sections) of the NCAT track. The

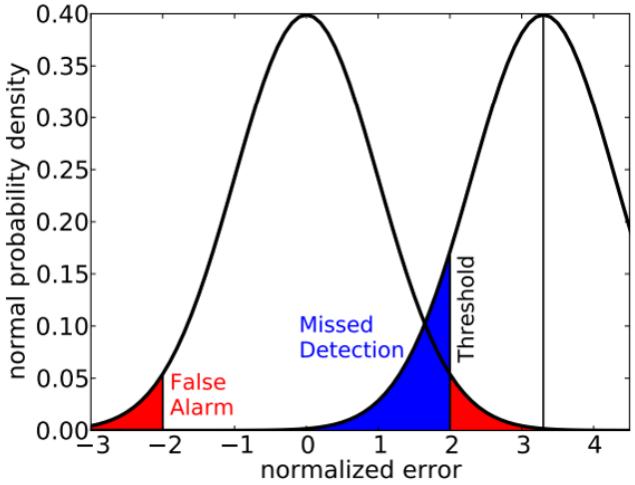

Figure 6.1: Fault Detection Example [12]

banked turns represent the greatest relative motion between the cabin and chassis. This result is as expected and confirms that the poor misalignment model causes biased measurements. Therefore, this fault detection method can be used to characterize other improved TA filters to ensure that measurements are not biased.

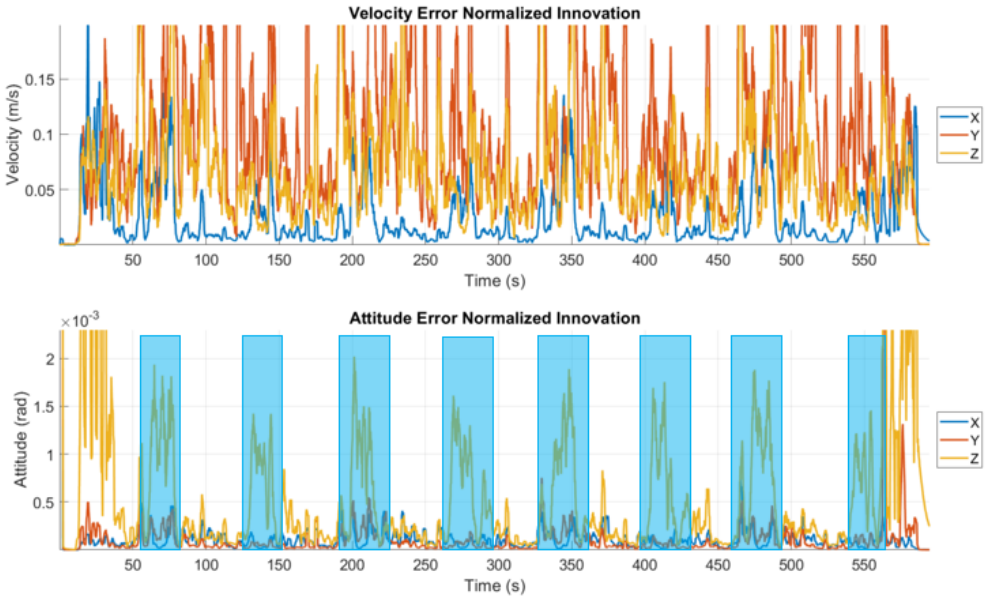

Figure 6.2: Initial NCAT Normalized Innovation Results

6.2 Rigidity Detection

The first approach to correcting the biased measurements is to only provide cabin measurement updates while the two bodies are considered rigid to one another. This way there would be no

need for a complex misalignment model. Instead, the two bodies could be considered static relative to one another. To accomplish this, a rigidity value can be arbitrarily created based on the difference of angular rate measurements between the cabin and chassis. This was shown to be successful in prior research where the rigidity detection to estimate static offsets between a foot-mounted IMU and a reference vehicle during a drive [1]. Figure 6.3 shows a simple diagram of the principal.

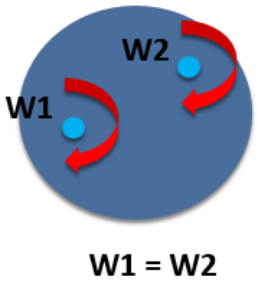

Figure 6.3: Rigid Body

If an object is rigid that means the magnitude of angular rates at every point on that object is the same. In the case of the cabin and chassis, the norm of the filtered angular rates on the cabin and chassis IMU can be compared to create a rigidity value (RV) representation of the rigidity between the two bodies using Equation (6.3).

$$RV = \left| \sqrt{\omega_{cab,x}^2 + \omega_{cab,y}^2 + \omega_{cab,z}^2} - \sqrt{\omega_{chassis,x}^2 + \omega_{chassis,y}^2 + \omega_{chassis,z}^2} \right| \tag{6.3}$$

A problem that arises from using the rigidity value, RV, is that although it is true that all points on a rigid object will experience the same magnitude of angular rate, it is also true that two objects can experience the same magnitude of angular rate and not be rigid to one another. Essentially, the cabin and chassis could be rotating in opposite directions, but at the same magnitude, and this would still be considered rigid.

Figure 6.4 shows the RV over the course of the NCAT track. As seen in the figure, the RV also increases where errors increased at certain turns, such as the East U-turn on the NCAT Track. However, the value remains under the set threshold for others turns, such as the West U-turn. The problem mentioned earlier occurs at the West U-turns; the magnitude of each

bodies change in attitude is similar even though the relative attitude between the two bodies is increasing. Thus, using the rigidity value will not always achieve the desired performance of restricting or preventing the biased measurements from affecting the final solution.

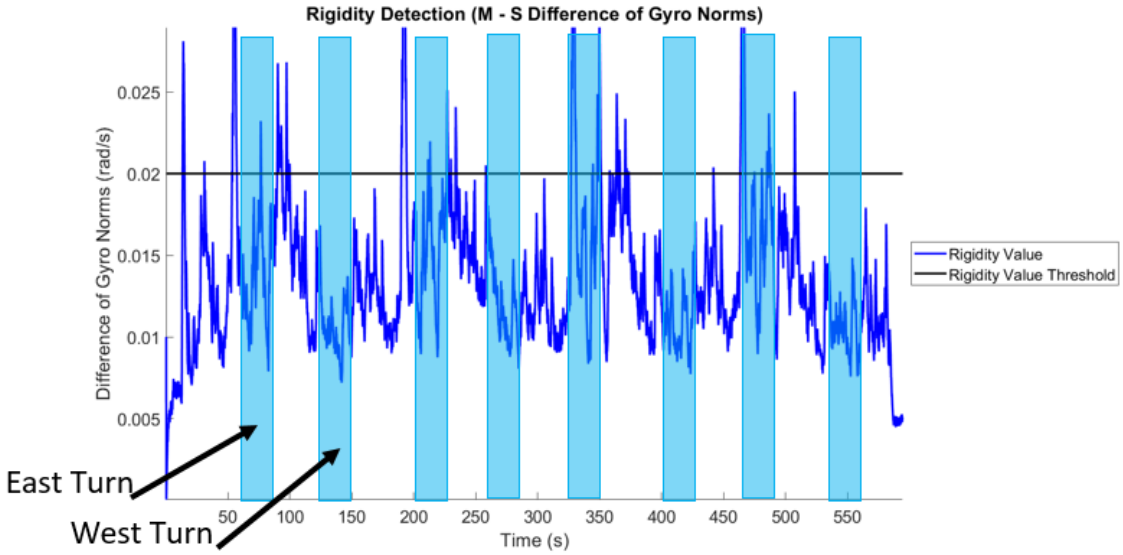

Figure 6.4: NCAT Track Rigidity Detection

6.3 Misalignment Models

The goal of the rigidity detection method is to remove the need for modelling the misalignment states. By only applying the cabin measurements when the two bodies were considered rigid to one another, then the original Dual GPS/INS methods rigidity assumption would be correct. However, the rigidity detection method was inconsistent – at times saying the two bodies were rigid when they were not. Therefore, the focus was shifted to exploring new methods for the dynamic model of the misalignment states. The following sections examine various models.

6.3.1 Higher Order Markov Model

A major field that uses transfer alignment to assist in the estimation of non-rigid bodies is aerospace. The plane body includes many sensors to create full attitude solutions, but the wing does not have the means to include additional sensors. However, wing mounted systems may need high accuracy attitude measurements. In these cases, different relative frequencies and oscillations experienced between the wing and plane body create difficulty in estimating the

relative attitude. This is because a simple model of the misalignment does not fit the actual motion. Research found that these different frequencies were regular enough to be successfully modelled using higher order Markov processes [19]. An example of a relative frequency response between the aircraft wing and body is shown in Figure 6.5. The aircraft experiences resistance from the air during flight that induces consistent patterns in frequency or constant frequencies that are readily identifiable. This characteristic makes this method very successful for this system, because the frequency responses can be directly translated into model parameters.

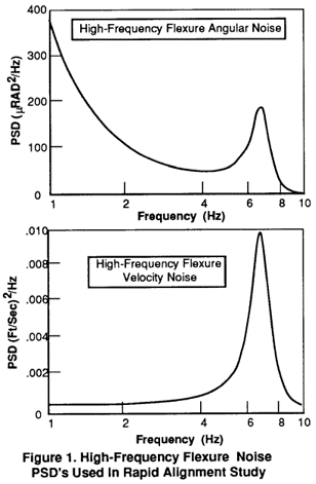

Figure 6.5: Example of Frequency Analysis [19]

In Chapter 5, the misalignment angles were modelled using a 1st-Order Markov model. However, this model was found to be overly simplistic. One improvement would be to determine if the relative motion between the cabin and chassis bodies were structured enough to be identifiable by its frequency response. However, the truck's relative motion is often related only to the route or road surfaces, which is highly variable. This can be seen when looking at the relative angles from the test performed on the NCAT track in Figure 3.6. In this figure, there are increases in relative motion during the banked turns of the track, highlighting that the misalignment between the two bodies is not a constant frequency but rather directly related to track position or the general dynamics of the truck. This fact makes higher order Markov processes not feasible for this problem.

6.3.2 Flexure States

When analyzing the frequency model, the semi-truck's relative motion between bodies was related more to the road surface and accelerations undergone by the truck than by the a constant frequency from vibration. A similar problem can occur in airplanes during a wing-rock maneuver. A wing-rock maneuver is a high acceleration turn shown in Figure 6.6. This maneuver creates relative motion between the wing and aircraft body that is non-oscillatory. To solve this issue, some suggest creating additional states to relate the relative accelerations between the two bodies and their misalignment angles [9].

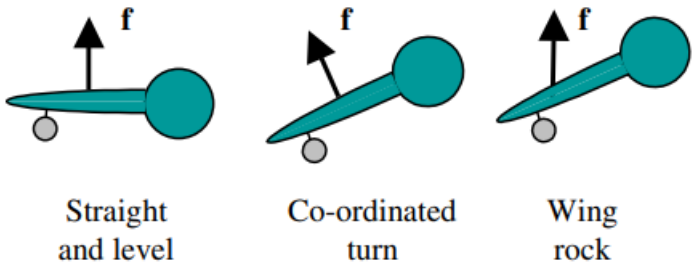

Figure 6.6: Wing Rock Example [9]

In a wing-rock maneuver, the misalignment between the wing and the body of the airplane is related to the motion of the airplane and is known as wing-flexure. Groves created additional states to estimate the wing-flexure [9]. These intermediate states related the acceleration the wing experiences to the misalignment between the two bodies, creating a correlation between the two that appears in the state transition matrix. Equation 6.4 shows an example of this implementation [9]. This works well for the aircraft's relative attitude estimation, because the aircraft experiences high accelerations during the wing-rock maneuver, making these additional states observable.

$$\Psi_r = \begin{bmatrix} \Psi_{rsx} \\ \Psi_{rsy} \\ \Psi_{rsz} \end{bmatrix} = \begin{bmatrix} 0 & \Psi_{fxy} & \Psi_{fxz} \\ \Psi_{fyx} & 0 & \Psi_{fyz} \\ \Psi_{fzx} & \Psi_{fzy} & 0 \end{bmatrix} \begin{bmatrix} f_x^b \\ f_y^b \\ f_z^b + g \end{bmatrix} \tag{6.4}$$

The wing-rock maneuver is similar to the motion experienced by the semi-truck but on a much higher acceleration scale. This solution can not be applied to the semi-truck system, because the semi-truck can not under go the appropriate amount of excitation to estimate the additional flexure states. Also, the semi-truck often has a worse ability to perform unique motions to gain the observability needed to properly estimate these states. Essentially, the filter is already unable to observe all current states, and the addition of more states will not make up for this error.

6.4 Measurement Noise related to Dynamic Motion

The previous section explored modifications to the state transition matrix as a means to mitigate the TA filter's biased measurement issue. However, these modifications need either readily identifiable parameters or high dynamic maneuvers to have states be fully observable. Both of these options were found to not be viable.

In this section, instead of modifying state transition matrix, the inertial dynamics of the semi-truck were applied to the measurement covariance. This technique was also similarly applied to aircraft that could not undergo appropriate amounts of acceleration to make states observable for the estimation of relative attitudes [9]. The actual excitation/inertial measurements are used as an input to a function for the measurement noise matrix. An equation to adjust the measurement noise matrix is represented by either Equation (6.5) or (6.6) showing that it could be based on the acceleration or the angular velocity.

$$R_{ta} = S_0 + S_1 \begin{bmatrix} a_{chassis,x} \\ a_{chassis,y} \\ a_{chassis,z} \end{bmatrix} + S_2 \begin{bmatrix} a_{chassis,x} \\ a_{chassis,y} \\ a_{chassis,z} \end{bmatrix}^2 ..... + S_n \begin{bmatrix} a_{chassis,x} \\ a_{chassis,y} \\ a_{chassis,z} \end{bmatrix}^n \tag{6.5}$$

$$R_{ta} = S_0 + S_1 \begin{bmatrix} \omega_{chassis,x} \\ \omega_{chassis,y} \\ \omega_{chassis,z} \end{bmatrix} + S_2 \begin{bmatrix} \omega_{chassis,x} \\ \omega_{chassis,y} \\ \omega_{chassis,z} \end{bmatrix}^2 ..... + S_n \begin{bmatrix} \omega_{chassis,x} \\ \omega_{chassis,y} \\ \omega_{chassis,z} \end{bmatrix}^n . \tag{6.6}$$

Unlike the previous potential updates which added additional parameters or states in the state transition model, this method only scales the measurement covariance. Therefore, there are no concerns about a decrease in observability of the states or a need to tune many parameters. This method is successful in removing the biased measurements, because it targets the measurement covariance matrix, R, from the fault detection analysis tool in Equation (6.2).

This method is also quite intuitive. During periods of high dynamics, it is expected that there will be more relative motion between the cabin and chassis, making the simple first order Markov model ineffective. When this model is ineffective, the incoming cabin measurement can not be properly related to the chassis attitude or the misalignment states. This method responds to the ineffective model by increasing the measurement covariance for the cabin measurement.

Figure 6.7 shows the normalized innovation values for the NCAT dataset where the measurement noise covariance is directly scaled with the dynamics of the chassis using Equation (6.5). There is a stark decrease in the normalized values compared to the previous Figure 6.2, where the fault detection method was originally derived. This change shows that this method can be reliable for removing the biased measurements.

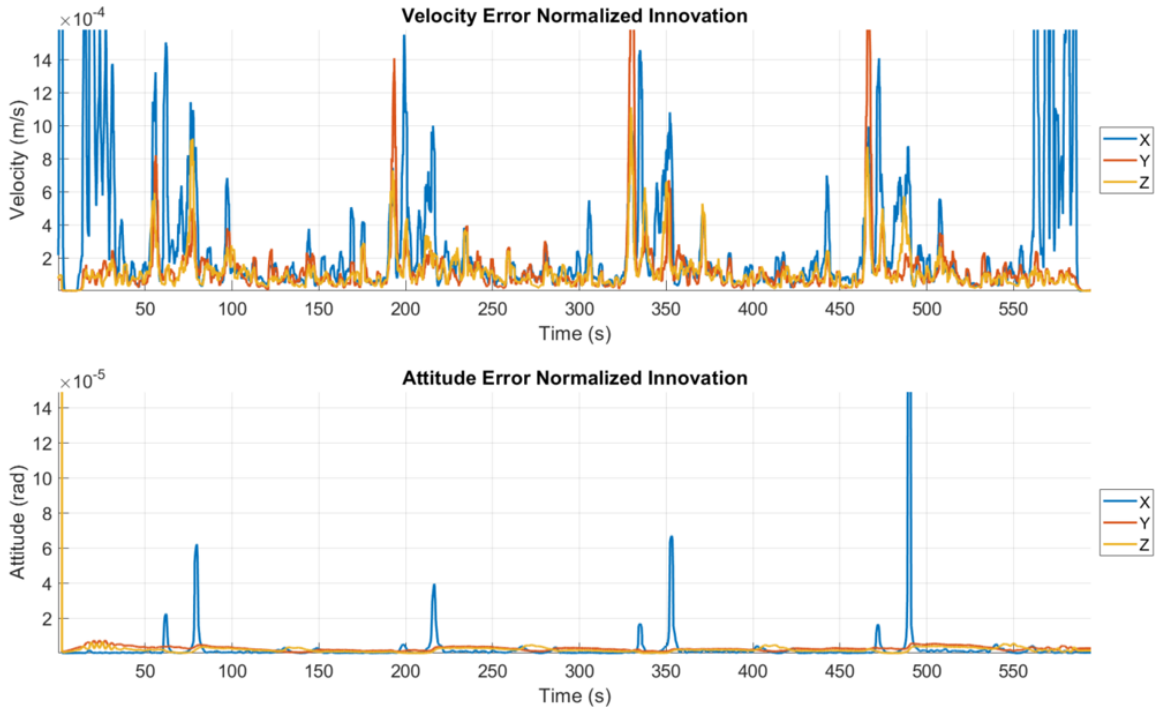

Figure 6.7: Updated NCAT Normalized Innovation Results

Chapter 7

Dynamic Transfer Alignment

In the previous chapter, potential solutions to the TA filter from Chapter 4 were explored. The original TA filter suffered from errors related to a poor misalignment model. The poor model would cause the incoming cabin attitude measurements to appear biased, potentially causing stability issues in the EKF. The previous chapter brought in the fault detection analysis tool to identify where these biased measurements occurred. A new method was found to remove these biased measurements by dynamically scaling the measurement noise covariance with the inertial measurements experienced by the chassis. This was shown previously to reduce the normalized innovation results from the NCAT track dataset and in doing so reduce the instability in the estimator. In this chapter, dynamic scaling of the measurement noise matrix will be fully integrated into the original TA filter and the results will be reviewed and analyzed.

7.1 Results

The original TA filter kept the attitude measurement noise covariance constant over the entire route. In this section, the attitude measurement noise covariance is dynamically changed using filtered accelerometer values from the chassis IMU. Figure 7.1 shows the cabin attitude measurement covariances over the course of the NCAT track dataset using Equation (7.1).

$$R_{ta} = S_0 + S_1 \begin{bmatrix} a_{chassis,x} \\ a_{chassis,y} \\ a_{chassis,z} \end{bmatrix} \tag{7.1}$$

This figure highlights changes in the cabin attitude covariance during the banked turns of the NCAT track, unlike previous filters where the covariances remained constant. Because the first order Markov model is least accurate during banked turns, the cabin attitude covariance will be increased to reflect that change.

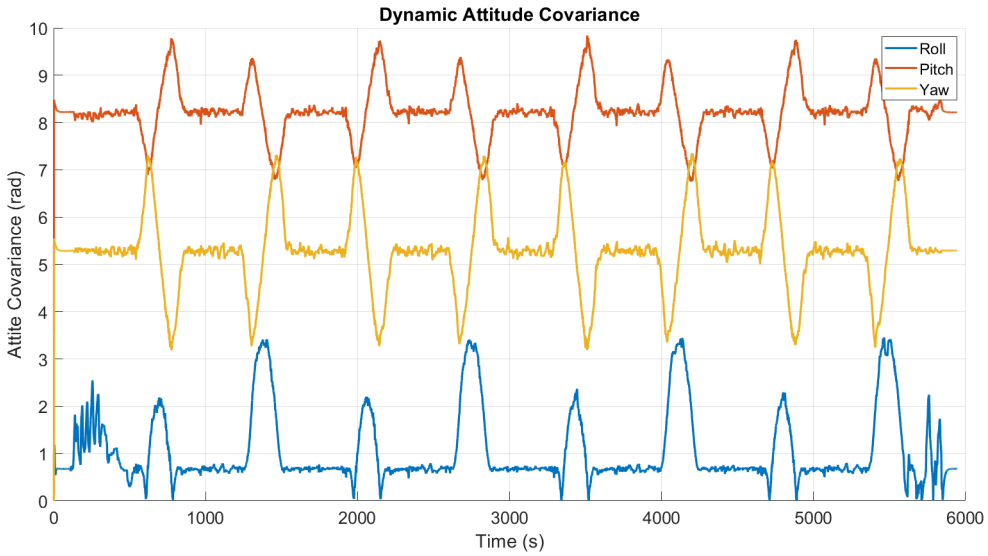

Figure 7.1: NCAT Dynamic Attitude Covariance

The inclusion of the dynamic measurement noise values has a large effect on the estimated chassis attitude covariances. Figure 7.2 shows the chassis attitude error state covariances from the NCAT dataset. In this figure, the error covariances are increased during the banked turns of the NCAT track. This is expected because there is an increase in acceleration. The original TA filter saw a large saw-tooth pattern from the stark difference in the prediction and update step covariances. However, in the Dynamic TA filter this magnitude has been decreased, ensuring that the chassis attitude will not overly replicate the now less helpful cabin measurement. Furthermore, now the misalignment states can be properly related to the incoming chassis measurements during periods of high relative motion.

This improvement in the misalignment states is evident in Figure 7.3 which graphs the misalignment angles estimated for the NCAT dataset. These estimates better represent the expected change in misalignment angles over time between the cabin and chassis body, because the misalignment angles now stay below the actual relative motion experienced. However, the results still include increases above the expected relative motion during the banked turns.

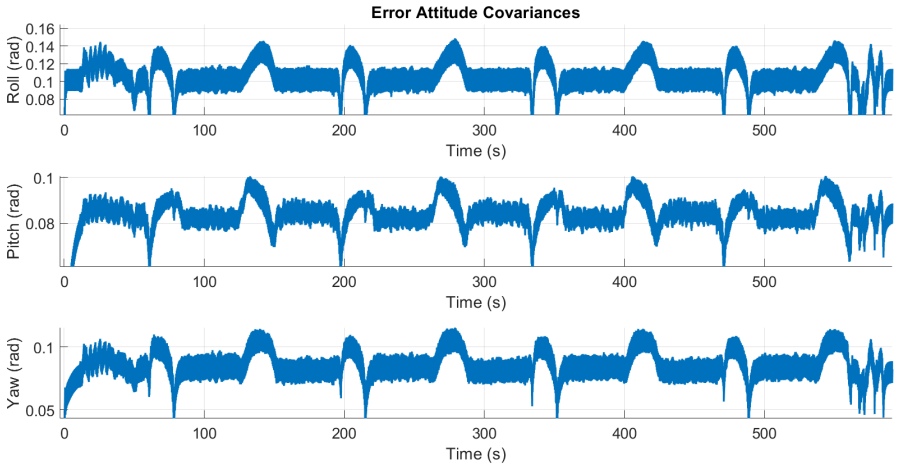

Figure 7.2: NCAT Updated Transfer Alignment Attitude Covariances

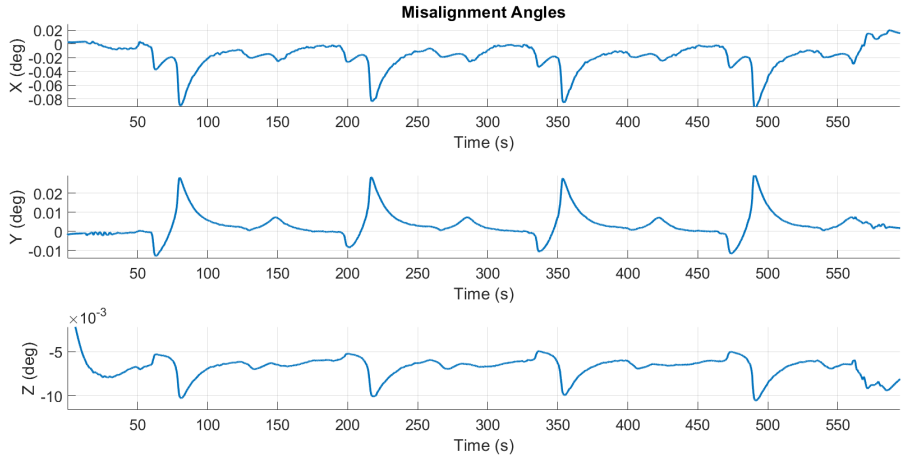

Figure 7.3: NCAT Updated Transfer Alignment Misalignment Estimates

Figure 7.4 plots the chassis attitude state error by comparing the Updated TA attitude results to the truth (chassis eTALIN) for the NCAT track dataset. The dynamic measurement noise matrix scaling drastically improved the solution in the roll and pitch angles. The magnitude of the error decreased from over 1.0 degree to under 0.5 degrees.

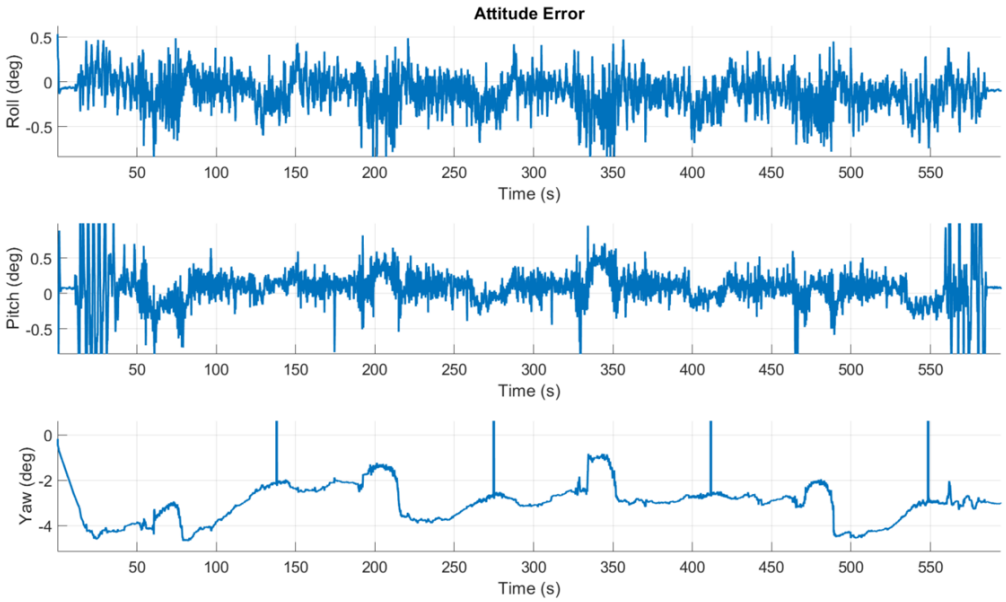

Figure 7.4: NCAT Updated Transfer Alignment Attitude Error Results

However, there is an increase in noise on both the roll and pitch angles results compared to the original TA filter. Furthermore, there are larger errors on the yaw angle estimate compared to the original TA filter. The increase in noise is expected because the filter is now trying to compensate for the poor misalignment model by increasing the covariance on the cabin measurements. This leads the filter to place more confidence on the poorer quality chassis IMU. Note that tuning of the dynamic measurement matrix scaling can create possible stochastic observability problems for the filter if the noise level of the solution is greater than the actual relative motion. The following section will explore this issue.

7.1.1 Dynamic TA Stochastic Observability

The Dynamic TA filter is able to keep the roll and pitch errors for the chassis attitude under the magnitude of relative motion that the truck experiences. However, there are increases in the noise of the solution during the turns of the NCAT track. This increased noise could be related

to the decrease in cabin attitude measurement confidence or to a lack of stochastic observability caused by a poor cabin sensor. If the incoming cabin attitude measurement confidence is too low, then the additional scaling of the measurement noise matrix could cause the filter to rely too heavily on the poor measurements from the sensor mounted on the chassis. On the other hand, the relative motion may be occluded by measurement noise, hidden beneath the noise floor. This would make estimation of the chassis attitude states impossible.

The stochastic observability describes whether the quality of an incoming measurement is detrimental to the estimation of states. In essence, the excitation a filter needs to estimate states may exist below the noise floor of the measurement. If this is the case than those states would become unobservable. In Figure 7.5, a lower performance sensor is used for the cabin attitude measurement for the Dynamic TA filter using the NCAT track dataset. This lower performance sensor has an attitude standard deviation of over 0.5 degrees, which means the noise level is often above the actual relative motion that is trying to be perceived by the filter. Therefore, the attitude error shown in the figure becomes mostly noise. The roll and pitch states have become unobservable with this lower performing sensor. Therefore, the cabin attitude solution needs to be good enough to handle an increase in the measurement noise matrix by dynamic scaling and keep the relative motion between the two bodies above the noise floor of its attitude.

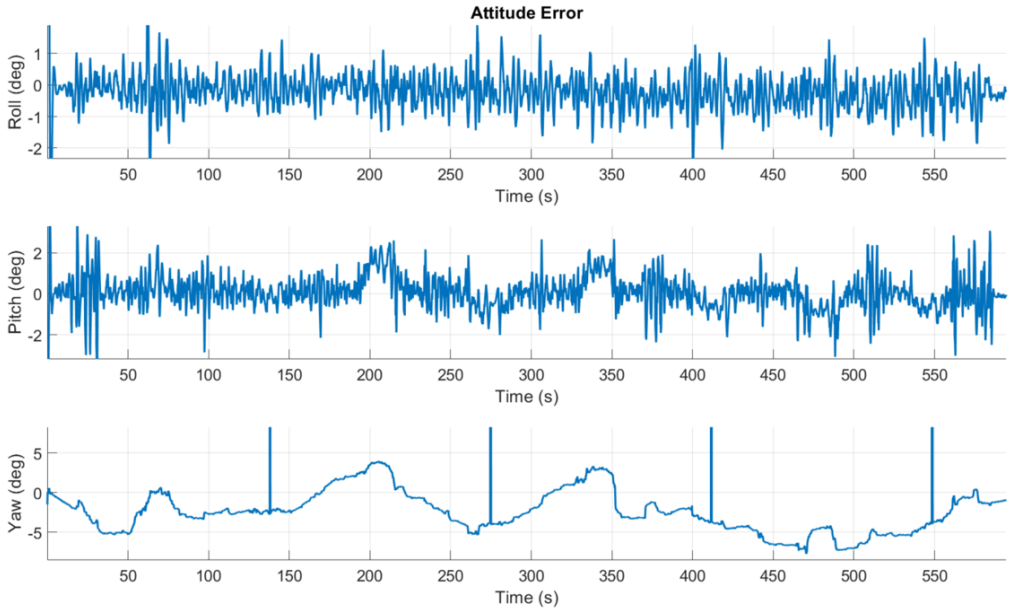

Figure 7.5: Stochastic Observability example when decreasing the quality of the reference system

7.1.2 Dynamic TA Deterministic Observability

Previously, there was an observability issue with the yaw estimate when using the original Dual GPS/INS method. The velocity measurement of the GPS receiver was related to the chassis attitude through the excitation, or change in acceleration, within the state transition matrix. However, the semi-truck did not experience enough lateral and vertical excitation to make the yaw angle observable. To mitigate this issue, the filter was modified to rely on both the velocity and attitude cabin measurements, rather than only the velocity measurement.

The addition of an attitude measurement also came with new states that needed to be estimated in the form of the misalignment angles. However, when the original transfer alignment was implemented, there was an over reliance on the cabin attitude. This caused the chassis attitude to replicate the cabin attitude, leading to minimal error in the yaw estimate because there is minimal misalignment between the cabin and chassis yaw angles. Originally, this appeared to be a good result, but it actually hid an observability issue that needs to be addressed.

Now that the filter scales the cabin measurement covariances, the once hidden deterministic observability issue is highlighted. The incoming attitude measurements are related to both the chassis attitude states and the misalignment angle states. To separate the states, the observation model uses the current estimate of the chassis attitude in the form of a rotation matrix. Figure 7.6 highlights the correlation between the attitude states and the incoming cabin measurements. To successfully separate these states, there needs to be enough excitation in the change in attitude rather than acceleration. Changing roll and pitch angles create enough excitation to observe the yaw attitude, but in the case of the NCAT track, there are very limited amounts of excitation in the pitch and roll angles. So, during straight line driving the yaw angle estimate drifts more compared to the turns, which often have spikes in the correct direction as seen previously in Figure 7.4.

Figure 7.7 shows the error between the chassis attitude estimates compared to truth (chassis eTALIN) for the Roads dataset. During periods of long straight driving in the Roads dataset, it can be seen that even the roll and pitch estimates suffer from a lack of excitation in the yaw angle. Both the roll and pitch estimates show large increases in error compared to the actual

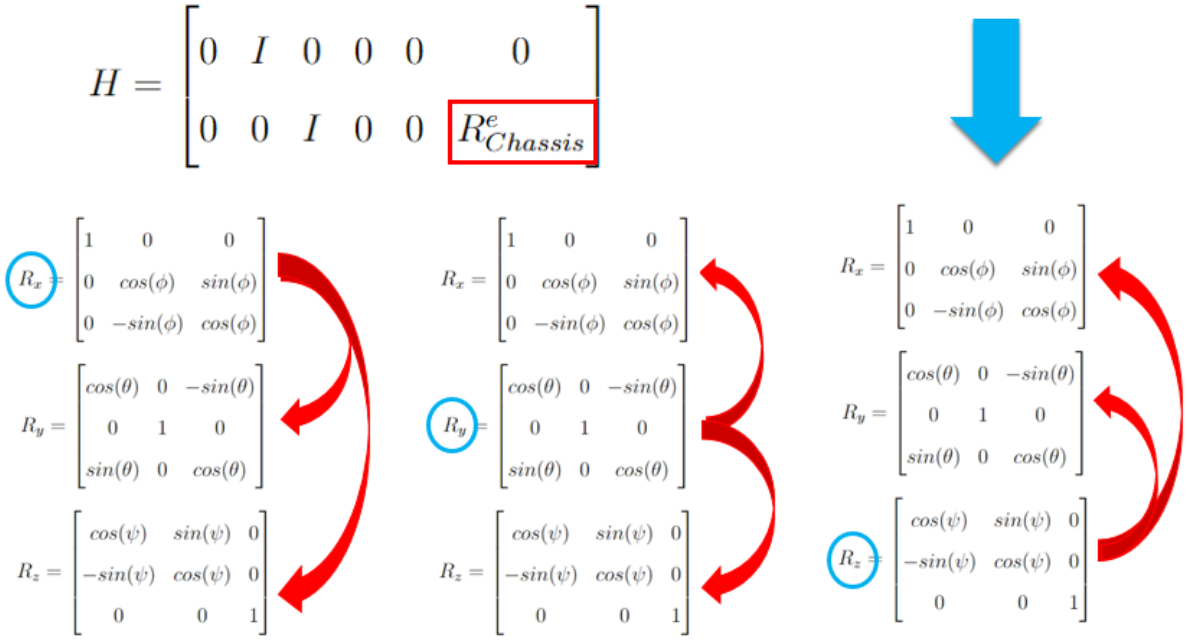

Figure 7.6: Deterministic Observability Diagram

relative motion experienced between the cabin and chassis. The error in the roll and pitch direction can be over a degree.

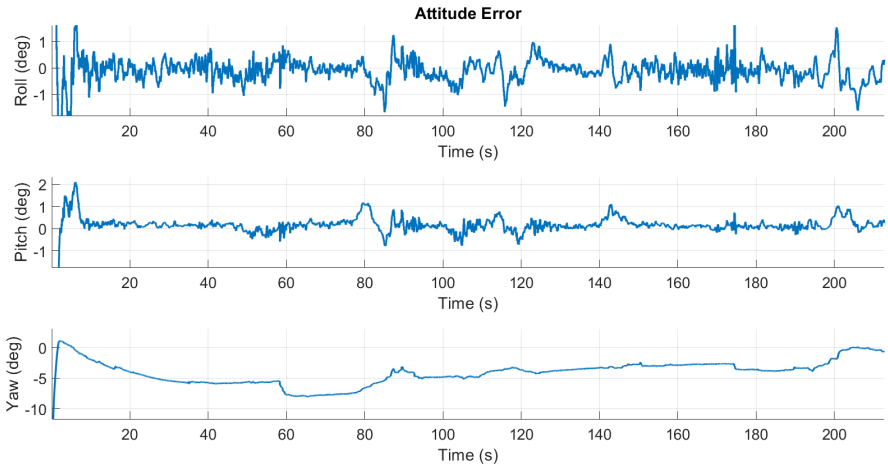

Figure 7.7: Roads Dataset Updated Transfer Alignment Attitude Error

Also, the Roads dataset is less dynamic than the NCAT track dataset. Having less dynamics limits the overall effectiveness of the Dynamic TA filter compared to the original filter. The measurement noise matrix is scaled over the entirety of the run, but there is not enough separation between the useful and poor cabin measurements. This leads to more reliance on the poor measurement from the chassis sensor which also leads to a more noisy final attitude

solution. This is an important design consideration because semi-trucks often drive highway routes that will have little overall excitation.

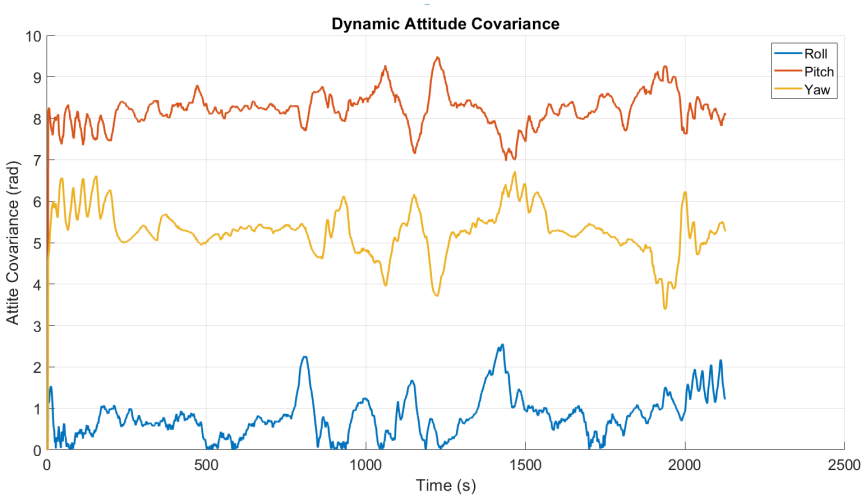

Figure 7.8: Roads Dynamic Measurement Noise

7.2 Results Analysis

The Dynamic TA filter was able to improve the results over the previous TA filter by removing the bias measurements caused by a poor misalignment model. These bias measurements in the TA filter would cause the best solution to overly replicate the incoming cabin measurements. Now, the Dynamic TA filter is able to better distinguish between the chassis attitude and misalignment angles from the cabin attitude information. This led to the attitude error having 0.4 degrees or less of standard deviation in the roll and pitch direction as well as a max error of only 0.6 degrees. These results were much improved compared to the TA filter which could see up to 1 degree of error.

However, there was a noticeable observability issue with the yaw angle states due to a lack of excitation that the vehicle experiences in the roll and pitch directions. This was shown to be true because of the use of the chassis attitude states in the observation model. The noise on the system was also larger due to increasing the measurement noise matrix during periods of relative motion, This is due to the filter utilizing the poorer quality sensor mounted on the chassis. The Dynamic TA filter performs well and helps to estimate the critical chassis attitude states, but still lacks adequate performance on the yaw angle. However, it should be noted that

this is less of a concern because the cabin and chassis don't often differ in the yaw direction. This leads to the development of a reduced-order Kalman filter shown in the next chapter.

Chapter 8

Reduced-Order Dynamic Transfer Alignment

The Dynamic TA filter is unable to observe the yaw angle, because the semi-truck does not experience enough excitation in the roll and pitch directions. The Dynamic TA filter linearizes the state transition and observation models around its current state estimates of the roll, pitch, and yaw angle. This can cause an issue when a state is unobservable, because the linearized approximation is worse. The roll, pitch, and yaw error states appear and are linearized in both the state transition and observation models. Therefore, the farther these states are from the truth, the more the filter will suffer with instability.

In all previous iterations of the filters, it has been a struggle to gain observability of the yaw angle. In the TA filter, the observability issue was not as apparent due to the tuning favoring the cabin measurement, which has a yaw measurement that is very similar to that of the chassis. In the Dynamic TA filter, the yaw angle is more obviously unobservable, because it is no longer biased by the cabin solution. This unobservable state is then being used to linearize the Kalman filter and update the covariances of the current states. However, the relative yaw angle between the chassis and cabin is small enough that there is potential to reduce the filter to not include the yaw as a state estimate and instead just use the yaw angle from the cabin measurement.

In this chapter, the Pure Reduced-Order Kalman filter [11] is applied to the system to remove the yaw angle from the estimated states. This method is also outlined by Brown, but the application to this EKF is described in [11]. Model reduction is applicable to the cabin-chassis relative estimation problem, because the relative yaw angle between the cabin and chassis is quite small, only around 0.1 degrees or less. To effectively reduce a system model, states need

to be considered known. In this instance, the yaw angle of the cabin can be considered equal to the chassis attitude.

Reducing the EKF should create improvement during periods of low excitation in the roll and pitch directions, because it will no longer be approximating the state transition using the unobservable yaw state. However, it should be comparable or possibly worse during periods of high dynamics, because of the invalid assumption of perfectly knowing the yaw angle state of the chassis.

8.1 Reduced Order Filter Design

The first step in reducing the system model is to partition the states that will be "eliminated" and the states that will be part of the "reduction". The letter E will represent states to be eliminated, and R will represent states that remain. The goal will be to essentially set the eliminated error states and their respective covariances to zero. It must also be ensured that the states and covariances do not change during the prediction or measurement updates. The new state transition and observation models can be re-written in terms of the reduced and eliminated parts as seen in Equations (8.1) and (8.2).

$$\begin{bmatrix} x_R \\ x_E \end{bmatrix}_{k+1} = \begin{bmatrix} \Phi_{RR} & \Phi_{RE} \\ \Phi_{ER} & \Phi_{EE} \end{bmatrix} \begin{bmatrix} x_R \\ x_E \end{bmatrix}_k + \begin{bmatrix} w_R \\ w_E \end{bmatrix}_k \tag{8.1}$$

$$z_k = \begin{bmatrix} H_R & H_E \end{bmatrix}_k \begin{bmatrix} x_R \\ x_E \end{bmatrix}_k . \tag{8.2}$$

Only the yaw error state will be a part of the eliminated states. This yaw error state and its respective covariance will remain zero, because there is the assumption that the yaw chassis state is completely known and matches the cabin yaw state. This requires the covariance matrix and process noise matrix to become zero where the yaw error states exists in the partition. The changes to states, covariances, and process noise are shown in Equations (8.3), (8.4), and (8.5), respectively.

$$x_k = \begin{bmatrix} x_R \\ x_E \end{bmatrix}_k \rightarrow \begin{bmatrix} x_R \\ 0 \end{bmatrix}_k \tag{8.3}$$

$$P_k = \begin{bmatrix} P_{RR} & P_{RE} \\ P_{ER} & P_{EE} \end{bmatrix}_k \rightarrow \begin{bmatrix} P_{RR} & 0 \\ 0 & 0 \end{bmatrix}_k \tag{8.4}$$

$$Q_k = \begin{bmatrix} Q_{RR} & Q_{RE} \\ Q_{ER} & Q_{EE} \end{bmatrix}_k \rightarrow \begin{bmatrix} Q_{RR} & 0 \\ 0 & 0 \end{bmatrix}_k . \tag{8.5}$$

The changes to the process noise matrix, covariance matrix, and the error states can now be applied to the different steps of the Kalman filter to keep the yaw error state and it's covariance at zero. Applying these updates to the Kalman gain equation in Equation (8.6).

$$\begin{aligned} K_{k+1} &= \begin{bmatrix} P_{RR} & 0 \\ 0 & 0 \end{bmatrix}_k \begin{bmatrix} H_R \\ H_E \end{bmatrix}_k \left(\begin{bmatrix} H_R & H_E \end{bmatrix}_k \begin{bmatrix} P_{RR} & 0 \\ 0 & 0 \end{bmatrix}_k \begin{bmatrix} H_R \\ H_E \end{bmatrix}_k + R_k \right)^{-1} \\ &= \begin{bmatrix} P_{RR} H_R (H_R P_{RR} H_R + R)^{-1} \\ 0 \end{bmatrix} = \begin{bmatrix} K_R \\ 0 \end{bmatrix}_{k+1} \end{aligned} \tag{8.6}$$

The above equation shows that the Kalman gain will remain zero at the eliminated states. This in turn will prevent the filter from updating the yaw error state and yaw error state covariance during the measurement update.

Considering the yaw angle to be equal to the cabin measurement means the rotation matrix that represents the attitude of the chassis must be rotated to match the yaw measurement when creating the attitude innovation. This rotation will act as the "subtraction" of the yaw error out of the system to maintain the zero yaw error state. This is analogous to estimating a bias in a voltage measurement. If a constant bias was completely know by a user of the device, it would be simpler for them to subtract the bias from the voltage measurement than it would be to estimate the bias through the use of a system model. The error states and error state

covariances are shown to keep the yaw error state angle zero during the measurement update given in Equation (8.7)

$$\begin{aligned} x_{k+1} &= \begin{bmatrix} x_R \\ 0 \end{bmatrix} + \begin{bmatrix} K_R \\ 0 \end{bmatrix} \left(z_k - \begin{bmatrix} H_R & H_E \end{bmatrix}_k \begin{bmatrix} x_R \\ 0 \end{bmatrix} \right) \\ &= \begin{bmatrix} x_R + K_R(z_k - H_R x_R) \\ 0 \end{bmatrix} = \begin{bmatrix} x_R \\ 0 \end{bmatrix}_{k+1} \end{aligned} \tag{8.7}$$

and the covariance update given in Equation (8.8) using the previously reduced Kalman gain form.

$$\begin{aligned} P_{k+1} &= \left(\begin{bmatrix} I_R & 0 \\ 0 & I_E \end{bmatrix} - \begin{bmatrix} K_R \\ 0 \end{bmatrix} \begin{bmatrix} H_R & H_E \end{bmatrix}_k \right) \begin{bmatrix} P_{RR} & 0 \\ 0 & 0 \end{bmatrix}_k \\ &= \begin{bmatrix} (I_R - K_R H_R) P_{RR} & 0 \\ 0 & 0 \end{bmatrix} = \begin{bmatrix} P_{RR} & 0 \\ 0 & 0 \end{bmatrix}_{k+1} . \end{aligned} \tag{8.8}$$

Finally, the time update of the covariance matrix must also keep the yaw error state at zero. The process noise matrix terms that deal with yaw error state will become zero. The resulting time update will use Equation (8.9).

$$\begin{aligned} P_{k+1} &= \begin{bmatrix} \Phi_{RR} & \Phi_{RE} \\ \Phi_{ER} & \Phi_{EE} \end{bmatrix} \begin{bmatrix} P_{RR} & 0 \\ 0 & 0 \end{bmatrix} \begin{bmatrix} \Phi_{RR} & \Phi_{RE} \\ \Phi_{ER} & \Phi_{EE} \end{bmatrix}^T + \begin{bmatrix} Q_{RR} & 0 \\ 0 & 0 \end{bmatrix}_k \\ &= \begin{bmatrix} \Phi_{RR} P_R \Phi_{RR}^T + Q_{RR} & 0 \\ 0 & 0 \end{bmatrix} = \begin{bmatrix} P_{RR} & 0 \\ 0 & 0 \end{bmatrix}_{k+1} \end{aligned} \tag{8.9}$$

Any user of a reduced order Kalman filter should note that this system makes a poor assumption compared to a typical EKF, because it assumes the yaw error state is completely

known with no variance, which is incorrect. During scenarios where there is proper excitation and observability, the reduced order filter will always perform worse than the original EKF. However, in this application, there is usually not enough pitch and roll excitation to make the yaw angle observable. Therefore, for most situations it is expected that the reduced order filter will produce comparable or better results.

8.2 Results

The Reduced-Order Dynamic TA filter aims to improve the Dynamic TA filter by removing the weakly observable yaw state. The dynamic measurement matrix scaling parameters were updated through experimentation to maximize the performance of the Reduced-Order Dynamic TA filter specifically for the NCAT track dataset. The new dynamic measurement covariance equation is shown in Equation (8.10).

$$R_{ta} = \begin{bmatrix} 2 \\ 2 \\ 0 \end{bmatrix} + \begin{bmatrix} 1.5 & 0 & 0 \\ 0 & 1.5 & 0 \\ 0 & 0 & 5e-5 \end{bmatrix} \begin{bmatrix} w_{chassis,x} \\ w_{chassis,y} \\ w_{chassis,z} \end{bmatrix} \tag{8.10}$$

The new cabin measurement attitude covariances are shown in Figure 8.1. This figure highlights a change in the dynamic scaling equation when compared to the Dynamic TA filter. Unlike previously, the roll covariance increases during the transition into banked turns, while the pitch angle covariance increased during the maximum change in the relative pitch angle. These differences are likely the effect of removing the yaw angle covariance.

Figure 8.2 shows the chassis attitude error for the NCAT track dataset. By assumption, the Reduced-Order Dynamic TA filter estimates a yaw angle that perfectly follows the cabin yaw angle. Therefore, the yaw error matches the relative motion from Figure 3.6. The roll and pitch errors in Figure 8.2 show slight spikes during the turn-straight transitions, as well as a 0.2 degrees steady state error. This steady state error is larger than any offset from the Dynamic TA filter shown previously in Figure 7.4. However, the white noise seen in the roll and pitch angles has greatly improved over the Dynamic TA filter now having a standard deviation of 0.2 degrees. This is likely due to the EKF no longer linearizing around an unobservable yaw error

state. Moreover, whatever noise that was introduced from the cabin's yaw measurement has been removed.

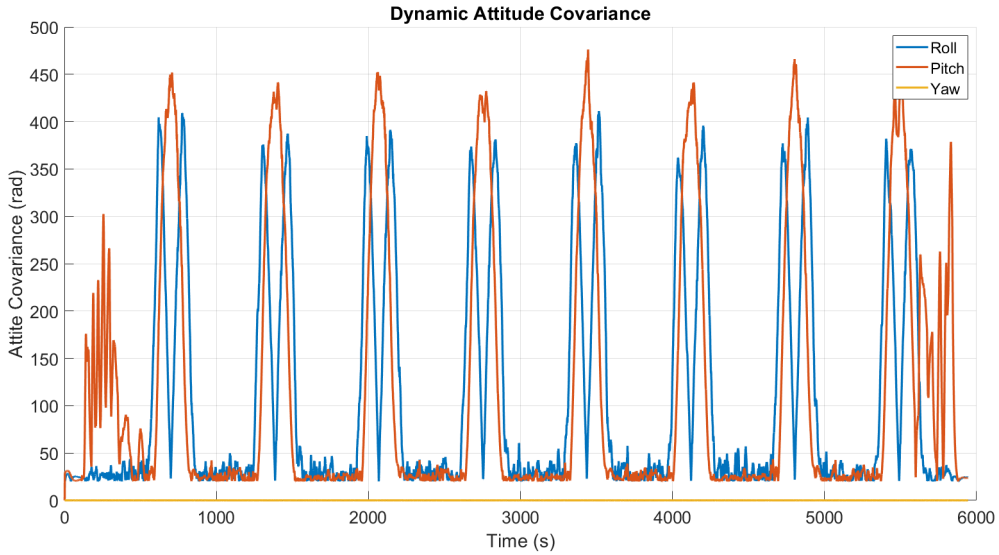

Figure 8.1: NCAT Dataset Model-Reduced Dynamic Measurement Covariance Scaling

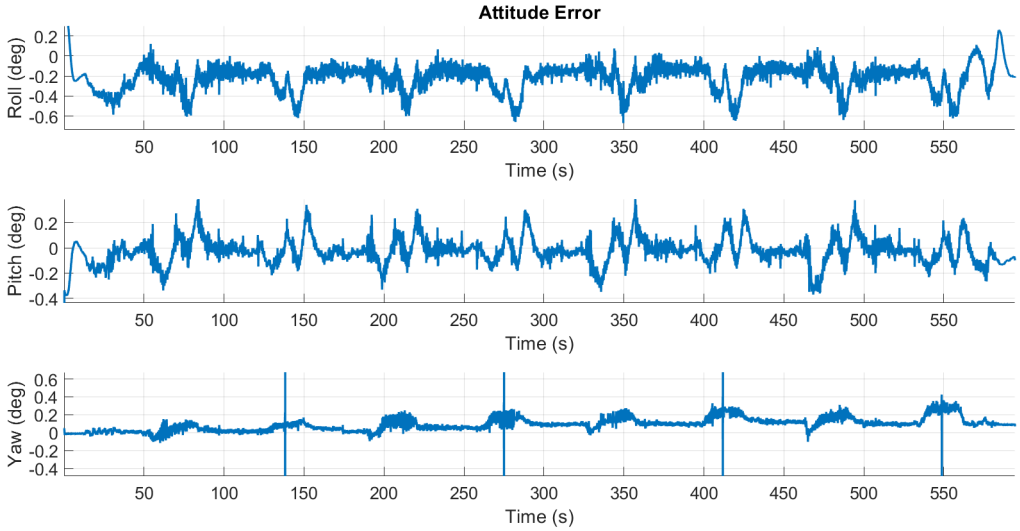

Figure 8.2: NCAT Dataset Model-Reduced Attitude Error

Previously, the dynamic measurement noise matrix scaled its values based on the motion of the vehicle. This allowed the filter to overcome some of the flaws of the poor misalignment angle model. A new problem occurs using the dynamic measurement noise with the Reduced-Order Dynamic TA filter. The dynamic measurement noise matrix still scales its values based on the total motion (x,y, and z axis) of the chassis. The chassis yaw motion can have effects on both the roll and pitch covariances. The reduced model may now improperly assign scaling,

because it still uses the yaw motion even though the Reduced-Order Dynamic TA filter has assumed this yaw motion is known perfectly. The dynamic measurement noise scaling was used to remove biased measurements, but it is no longer able to be properly applied to the reduced order model because of the faulty assumptions of the Reduced-Order Dynamic TA filter.

Figure 8.3 highlights this problem by plotting the normalized innovation for the NCAT dataset using the Reduced-Order Dynamic TA filter. There is an increase in overall magnitude compared to updated non-reduced transfer alignment in Figure 6.7. This confirms that biased measurements are being used for updates in the Reduced-Order Dynamic TA filter. Also, Figure 8.4, which plots the misalignment angles using the Reduced-Order Dynamic TA filter, now do not converge, likely due to the biased measurements from the cabin.

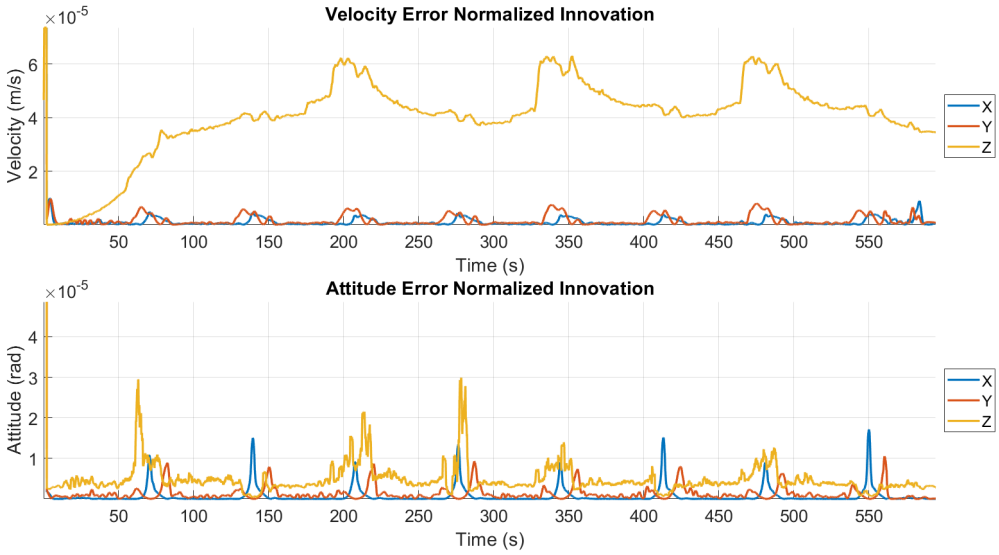

Figure 8.3: NCAT Dataset Model-Reduced Stability Concerns: Fault Detection

The measurements may also become biased because the reduction removes the covariance connection where the yaw error state covariance is typically related to the other two angles within the state transition matrix. Figure 8.5 graphs the attitude state covariance over time where the yaw angle now maintains zero, because the filter now considers it to be known. This is a good estimate because there is little change in the relative yaw angle. The shape of the roll and pitch angles are also now different compared to the Dynamic TA filter.

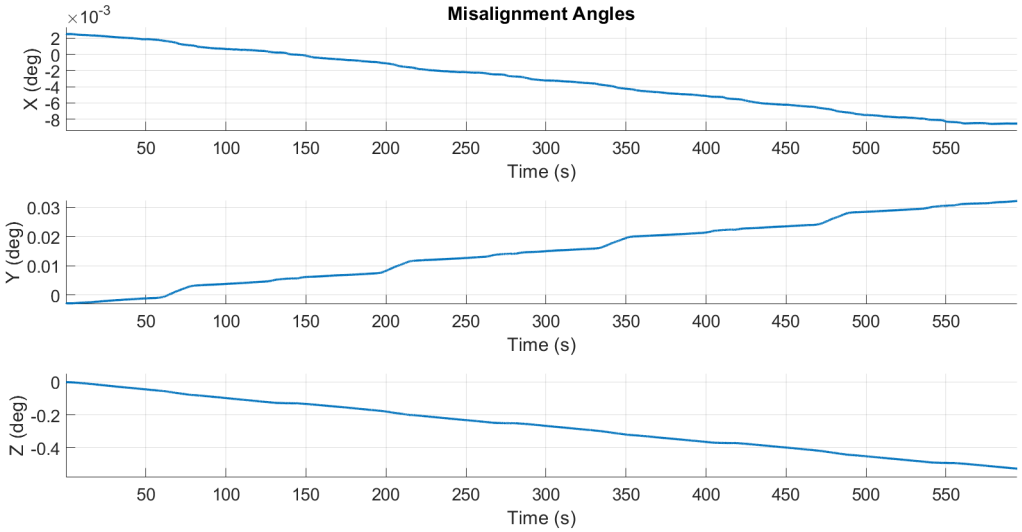

Figure 8.4: NCAT Dataset Model-Reduced Stability Concerns: Misalignment Angles

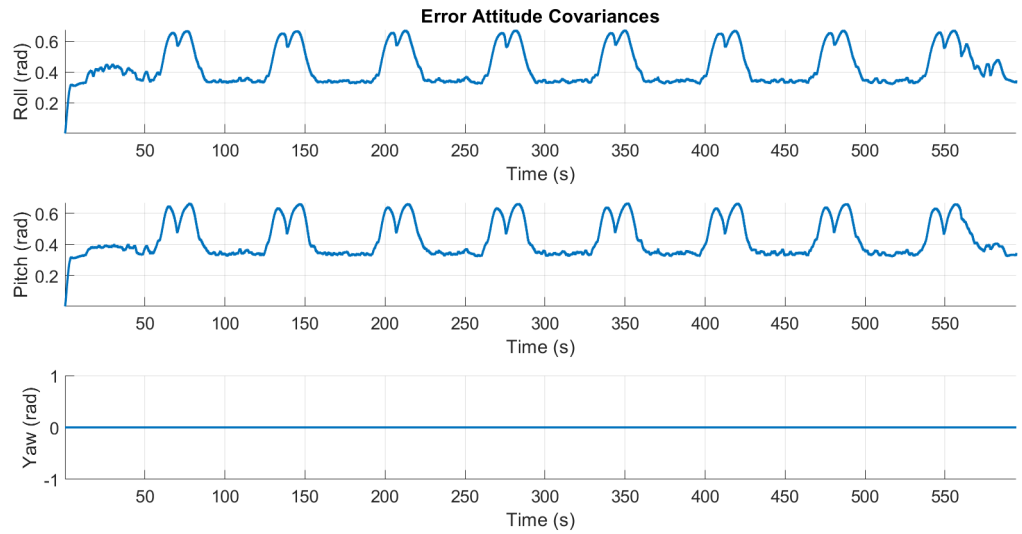

Figure 8.5: NCAT Model-Reduced Updated Transfer Alignment Attitude Covariances

These errors, however, are not as large in the Roads dataset. Figure 8.6 has the attitude errors for the chassis states for the Roads dataset. When analyzing the Roads dataset, an increase in performance can be seen over just the updated transfer alignment method in the roll direction from Figure 7.7. This roll error has a bias of around 0.2 degrees and a standard deviation of 0.2 degrees which is better than the previous non-reduced result which was experiencing roll error above 1.0 degree.

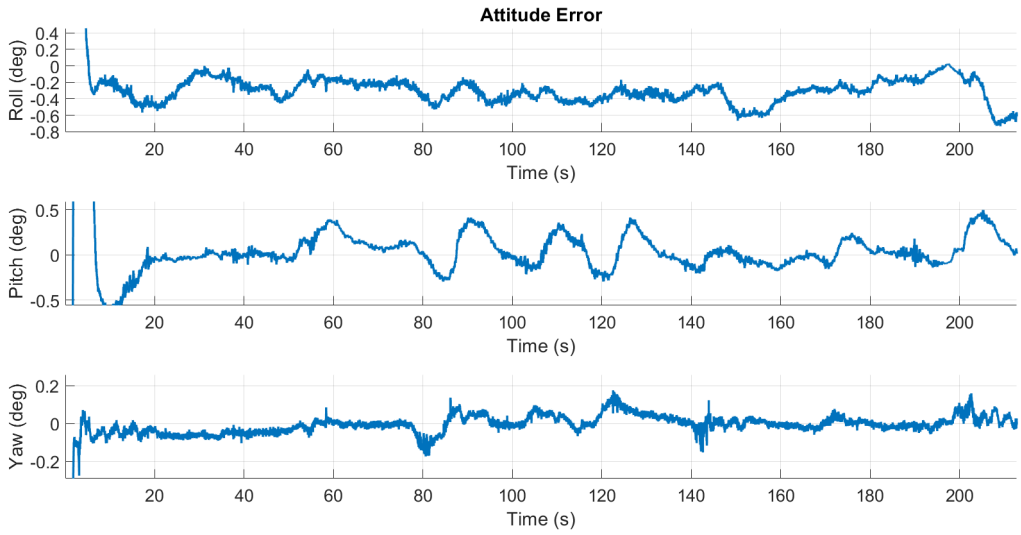

Figure 8.6: Roads Model-Reduced Attitude Error

The Roads dataset was able to benefit more from the reduced model because it experiences even less change in the roll and pitch directions compared to the NCAT dataset. This means that the dynamic measurement noise scaling more accurately represented the roll and pitch covariances and there was less of a connection between the yaw attitude error and the roll and pitch errors. Figure 8.7 displays the misalignment states for the Roads dataset. The reduced relative motion between the cabin and chassis led to the ability of the roll and pitch misalignment angles to converge compared to the NCAT dataset.

In this chapter, the Reduced Order Dynamic TA filter showed improvement over the Dynamic TA filter by limiting the amount of white noise in the estimates of the chassis roll and pitch angles. However, there were still some problems with the dynamic measurement scaling which uses all the inertial measurements experienced by the chassis, including the yaw motion.

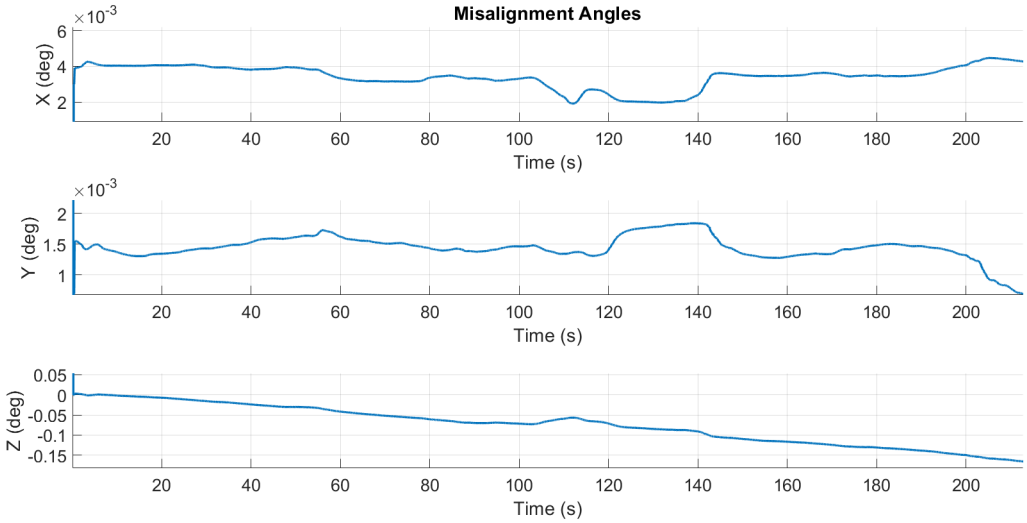

Figure 8.7: Roads Reduced Misalignment Angles

Also, the yaw error state covariances were disconnected from the roll and pitch error covariances within the state transition matrix. Both of these changes led to spikes in error and a steady state offset from the actual roll and pitch estimates. However, these errors were minimal compared to the white noise reduction seen compared to the Dynamic TA filter. This was especially true in the Roads dataset which benefited more because of its minimal excitation in the roll and pitch directions compared to the NCAT track. Meaning for most semi-truck driving scenarios this method would improve the chassis roll and pitch estimation over the Dynamic TA filter.

Chapter 9

Conclusions and Future Work

9.1 Conclusions

This thesis explored four main methods to estimate the relative motion between the cabin and chassis of a semi-truck. Knowing the relative motion is important for autonomous semi-trucks, because perception sensors are often mounted on the cabin and anything detected by them would appear offset to the chassis. The offset could critically affect different autonomous algorithms, such as path planing and control.

The relative motion between the cabin and chassis includes a complex suspension system. Therefore, any model used would need to have many parameters (spring/damper coefficients, torsion bars, etc.) that the user would need to know or estimate, which may require additional sensors. The goal of this thesis was to estimate this motion with a simpler model using sensors that would already be included on an autonomous semi-truck. The only sensors used in the thesis were two IMUs, one mounted on each body, and a GPS antenna mounted on the cabin.

The first method, Dual GPS/INS introduced in Chapter 4, used only the GPS antenna as a measurement update for the chassis IMU. This filter estimated the chassis IMU biases, which were used to correct the chassis attitude solution. However, this method had two main issues. First, because of the lack of excitation the semi-experienced in the longitudinal and lateral directions, the filter suffered from a lack of observability of the yaw state. The second major flaw of the Dual GPS/INS filter was the assumption that the GPS measurements were at a constant offset to the chassis IMU. This assumption led to increases in attitude errors during

the banked turns of a test track, where the difference between the GPS antenna and the chassis IMU were the largest.

A Transfer Alignment (TA) filter was proposed in Chapter 5 as an improvement to the Dual GPS/INS method. The TA filter added an attitude measurement from a combined cabin GPS/IMU filter solution and included additional misalignment states. The new attitude measurement was needed to address the lack of observability of the yaw angles, while the misalignment states were used to remove the constant offset assumption between the cabin and chassis. However, the chosen misalignment model was shown to be incorrect, causing the incoming attitude measurements to appear biased. Therefore, in areas of a track where there was increased relative motion, there was an increase in error for the chassis attitude results. These biased measurements, in turn, caused the best tuning for the filter to be one that overly matched the chassis attitude to the cabin attitude measurement.

Fault detection was then added for detecting the biased measurements caused by the poor misalignment model in the original TA filter in Chapter 6. This tool was then used to validate potential improvements to the misalignment model. Multiple improvements were considered to attempt to overcome the problems of the TA filter on the semi-truck. This thesis first looked at the possibility of detecting the rigidity (constant angular offset) between the cabin and chassis as a potential way of simplifying the misalignment model to a constant offset. However, the rigidity value lacked consistency and did not always align with zero relative motion portions of the datasets. Improving the model with a higher fidelity frequency model was also considered. This model also did not work, because it expected the semi-truck to experience constant frequencies of lateral and longitudinal acceleration between the two bodies which is not the case. Additionally, a method that added states to represent the flexure between the two bodies was investigated. However, this method struggled to be applied on the semi-truck because there was not ample excitation or acceleration to estimate the relative attitude.

The proposed solution that successfully estimated the chassis attitude was using a dynamically changing measurement noise matrix based on the accelerations and angular rates experienced by the chassis. Intuitively, the cabin measurements should be worse for the chassis solution under high dynamics because of the system lag that exists between the two bodies due

to the suspension system. This lag would induce a large magnitude of misalignment. Applying the fault detection tool to this Dynamic TA filter with dynamically changing measurement noise validated that there were less biased measurements from the cabin. The Dynamic TA filter was shown to keep the chassis roll error under 0.5 degrees and the pitch error around 0.3 degrees, which could be used to improve the solution of the relative motion between the cabin and chassis. However, the Dynamic TA filter still could not properly observe the yaw angle due to the lack of excitation a semi-truck experiences in the roll and pitch directions. This reliance was due to the form of the observation matrix which related the cabins attitude measurement to chassis attitude and the misalignment between states. This required attitude excitation to properly observe both the misalignment and the chassis attitude as shown in Chapter 7.

The Reduced-Order Dynamic TA filter was then used to remove the mostly unobservable yaw state from the system in Chapter 8. The estimator was able to be reduced because the relative yaw angle between the cabin and chassis remains small throughout the entirety of every dataset. This allowed the yaw estimate of the chassis to be completely replaced by the cabin yaw angle measurement. This solution brought down the noise of the system to be around 0.2 degrees standard deviation for both the chassis roll and pitch angle. However, this estimator created a steady state error due to the Reduced-Order Dynamic TA filter having the fundamentally worse assumption that the chassis yaw state is already perfectly known, compared to it being estimated in the Dynamic TA filter.

The relative motion between the cabin and chassis can be as high as 1.5 degrees. The work in this thesis showed that the chassis roll and pitch angles could be estimated within an accuracy of 0.2-0.5 degrees and only have 0.1-0.3 degrees of standard deviation on the chassis body. Additionally, multiple potential improvements were investigated and evaluated. While these methods are traditionally used on higher dynamic aerospace systems, this thesis found that they could be applied to a less dynamic ground vehicle setting and be beneficial. This is especially relevant, because these results could be applied to other ground vehicles that experience more excitation, such as off-road vehicles.

9.2 Future Work

The main problem as discussed above is that the semi-truck does not experience very dynamic motion and the motion it does experience is hard to properly model. To further the work of this thesis it will be important to explore the following ideas in future research:

- Using a simulation tool to be able to truly test a wide breath of reference unit and IMU qualities to determine optimal performance.
- Constraining the error growth of unobservable attitude states by applying inequality constraints to an extended Kalman filter. The semi-truck has a maximum possible misalignment offset that could be used to constrain the error growth seen in the yaw direction.
- Experimenting with more modelling techniques for the misalignment angles such as examining the frequency of the change in misalignment as well as attempting to use a simplified spring/damper model.
- The system should be able to benefit from an adaptive Kalman filter that weights multiple Kalman filters such as Multiple-Model Adaptive Estimation (MMAE). A range of different models could be effectively weighted against each other to determine an optimal solution. This could be beneficial if a model performs better during less excitation than another model which may perform better during high excitation.

References

[1] Thopay, Archit, "Initialization of a Pedestrian Navigation System Using a Transfer Alignment Approach" Auburn University, Alabama, 2020.

[2] Agnas, Edvin and Marcus Jerenvik, "Estimation of position and orientation of truck kinematic frames", Master Thesis, Chalmers University of Technology, Sweden, 2016.

[3] He, Shuilong, Keren Chen, Enyong Xu, Mingsong Ye, and Yanxue Wang. "Coupling analysis and optimization of commercial vehicles cab comfort with multi-platform integrated calculation." Journal of Mechanical Science and Technology 35, no. 10 (2021): 4329-4341.

[4] "Optimal State Estimator Algorithm — Understanding Kalman Filters, Part 4" Youtube, uploaded by MATLAB, 20 April 2017, https://youtu.be/VFXf1lIZ3p8

[5] "Nonlinear State Estimators — Understanding Kalman Filters, Part 5" Youtube, uploaded by MATLAB, 17 May 2017, https://youtu.be/Vefia3JMeHE.

[6] Graham, William, and Kevin Shortelle. "Advanced transfer alignment for inertial navigators (A-TRAIN)." In Proceedings of the 1995 National Technical Meeting of The Institute of Navigation, pp. 113-124. 1995.

[7] Groves, Paul D., and Jonathan C. Haddock."An all-purpose rapid transfer alignment algorithm set." In Proceedings of the 2001 National Technical Meeting of The Institute of Navigation, pp. 160-171. 2001.

[8] Groves, Paul D."Optimising the transfer alignment of weapon INS" The journal of Navigation 56, no. 2 (2003): 323-335.

[9] Groves, Paul D., Genevieve G. Wilson, and Christopher J. Mather. “Robust rapid transfer alignment with an INS/GPS reference.” In Proceedings of the 2002 National Technical Meeting of The Institute of Navigation, pp. 301-311. 2002.

[10] Groves, Paul D., ”Principles of GNSS, Inertial, and Multisensor Integrated Navigation Systems” Artech House, 2013

[11] Brown, Robert, and Patrick Hwang. ”Introduction to Random Signals and Applied Kalman Filtering, 4th edition” John Wiley Sons. Inc, 2012.

[12] Benjamin J. Clark. Fault Detection and Exclusion in Deeply Integrated GPS/INS Navigation. PhD Dissertation, Auburn University, December 2012.

[13] J. A. Farrell, F. O. Silva, F. Rahman, and J. Wendel, ”IMU Error State Modeling for State Estimation and Sensor Calibration: A Tutorial” 6 May 2019.

[14] ”IEEE Standard Specification Format Guide and Test Procedure for Single-Axis Interferometric Fiber Optic Gyros,” in IEEE Std 952-1997 , vol., no., pp.1-84, 24 Feb. 1998, doi: 10.1109/IEEESTD.1998.86153.

[15] Joon, Lyou, and Lim You-Chol. “Transfer alignment considering measurement time delay and ship body flexure.” Journal of Mechanical Science and Technology 23, no. 1 (2009): 195-203.

[16] Kain, James, and James Cloutier. “Rapid transfer alignment for tactical weapon applications.” In Guidance, Navigation and Control Conference, p. 3581. 1989.

[17] Rogers, Robert. “Velocity-plus-rate matching for improved tactical weapon rapid transfer alignment.” In Navigation and Control Conference, p. 2783. 1991.

[18] Schneider, Alan M. “Kalman filter formulations for transfer alignment of strapdown inertial units.” Navigation 30, no. 1 (1983): 72-89.

[19] Spalding, Kevin. “An efficient rapid transfer alignment filter.” In Astrodynamics Conference, p. 4598. 1992.

[20] Sutherland Jr, Arthur A. ”The Kalman filter in transfer alignment of inertial guidance systems.” Journal of Spacecraft and Rockets 5, no. 10 (1968): 1175-1180.

[21] ”National Statistics.” NHTSA. US Department of Transportation. https://www-fars.nhtsa.dot.gov/Main/index.aspx. 11/12/2022.

[22] Costello, Bob, and Alan Karickhoff. ”Truck Driver Shortage Analysis 2019.” ATA. July 2019. https://www.trucking.org/sites/default/files/2020-01/ATAs

[23] ”New Research Finds TuSimple Trucks are at Least 10 percent More Fuel Efficient Than Traditional Trucks Per TuSimple and UC San Diego Study” TuSimple. Dec 2019. https://www.tusimple.com/wp-content/uploads/2021/01/UCSD-Fuel-Study-Press-Release.pdf.

[24] Weisbrot, Eric. ”40+ Must-Know Trucking Industry Statistics” Freight Broker Bonds. JW Surety Bonds. January 2021. https://www.jwsuretybonds.com/blog/trucking-industry-statistics